19 Polybenzimidazoles*

Yan Wang, Tingxu Yang, Kayley Fishel,
Brian C. Benicewicz, and Tai-Shung Chung

CONTENTS

19.1 Introduction 618
19.2 Synthesis 619
19.2.1 General Route 619
19.2.2 Speci c Case for PBI 619
19.2.3 Product Requirements and Catalyst Effects 621
19.2.3.1 Requirements 621
19.2.3.2 Catalyst Effects 622
19.3 PBI Fiber Formation 622
19.3.1 Dope Preparation 622
19.3.2 Dry-Spinning Process 623
19.3.3 Hot Drawing 624
19.3.4 Sulfonation and Stabilization 624
19.4 PBI Blend Fibers 624
19.4.1 PBI/PI Blends 624
19.4.2 PBI/PAr Blends 627
19.4.3 PBI/HMA 631
19.4.4 PBI/PSF Blends 635
19.4.5 PBI/PAI Blends 636
19.4.6 PBI/PVPy Blends 637
19.5 Molded PBI Parts 637
19.6 PBI Matrix Resins and Composites 640
19.7 PBI Applications in High-Temperature Polymer Electrolyte Membrane Fuel Cells 640
19.7.1 Low versus High Operational Temperature for PEM Fuel Cells 640
19.7.1.1 PBIs for High-Temperature PEM Fuel Cells 641
19.7.1.2 Preparation of PBI–Acid Membranes 641
19.7.2 Impact of Chemistry on Fuel Cell Performance 643
19.7.2.1 Meta-PBI 643
19.7.2.2 Para-PBI 645
19.7.2.3 AB-PBI 648
19.8 PBI-Based Membranes for Pervaporation Separation 649
19.8.1 PBI-Based Membranes with Various Modi cations 650
19.8.1.1 Cross-Linking 650
19.8.1.2 Sulfonation 651
19.8.1.3 Polymer Blending 652
19.8.1.4 Mixed-Matrix Membranes 652
19.8.2 PBI Hollow Fiber Membranes 653

* Based in parts on the rst-edition chapter on polybenzimidazoles.

© 2016 by Taylor & Francis Group, LLC

19.9 PBI-Based Membranes for Gas Separation 654
19.9.1 Monomer-Level Optimization 654
19.9.2 N-Substitution Modi cation 657
19.9.3 Chemical Cross-Linking 657
19.9.4 Polymer Blending 657
19.9.5 Mixed-Matrix Membranes 657
19.10 Current PBI Products 659
Acknowledgments 660
Abbreviations 660
References 662

19.1 INTRODUCTION

Vogel and Marvel [1] synthesized the rst aromatic polybenzimidazoles (PBIs) in 1961. Because this polymer showed exceptional thermal and oxidative stability, National Aeronautics and Space Administration (NASA) and Air Force Material Laboratory sponsored DuPont and Hoechst Celanese to undertake fundamental research works on this material in the early stages of the development for aerospace and defense applications. Before the 1980s, major applications of PBI were in re-blocking applications, thermal protective clothing, and reverse osmosis (RO) membranes. Its applications became diverse by the 1990s; molded PBI parts and microporous membranes were developed. The former exhibited superior performance as sealing elements in high-temperature corrosive environments. Hoechst Celanese commercialized PBI in 1983. Today, PBI Performance Products Inc. (http://www.pbiproducts.com/) is the major producer of high-performance PBI materials.

Many authors have reviewed the general chemistry and historical development of various PBI polymers [2–8]. Lee et al. [2] and Frazer [3] summarized the early chemistry work on PBIs before 1968 and their applications as adhesives in composites. Neuse [4] extended Lee et al.'s work and included molded PBI parts and PBI membranes. Powers and Serad [5] and Buckley et al. [6] gave in-depth historical reviews on PBI syntheses, properties, and applications of PBI bers. They provided detailed information about the needed purities of monomers and ow charts for a large-scale production of PBI resins and bers. Cassidy [7] and Critchley et al. [8] studied polycondensation reactions of various PBIs and emphasized the use of PBI for aerospace composites and adhesives. They also investigated PBI thermal degradation. Jaffe et al. [9] reviewed the previous work on miscible PBI blends, whereas Choe [10] summarized the effects of various catalysts on PBI polymerization. Since the early twentieth century, PBI has been extensively used in high-temperature fuel cell applications, and several reviews have summarized its applications in this aspect [11–15]. A comprehensive review of PBI on its historical development and future R&D was given by Chung [16] in 1997. A review on its synthesis, properties, processing, and applications was also conducted by Dang et al. [17] recently.

In short, PBIs are a class of high-performance heterocyclic polymers, typically synthesized from a condensation reaction of aromatic bis-*o*-diamines and dicarboxylates. Benzimidazole moiety is the repeating unit in the polymer molecular backbone. Poly(2,2′-(*m*-phenylene)-5,5′-bibenzimidazole) is the only commercially available polybenzimidazole. This composition was chosen due to the fact that it had an extremely high glass transition temperature (T_g) of 425–435°C and a superior ame resistance. Since it did not burn and could not produce much smoke, its early marked focus was for the defense industry as high-value-added re-blocking materials and thermal protective clothing. PBI was the acronym for this composition. This material cost about $40/lb. in 1988 [18].

One of the objectives of PBI alloys is to tailor existing expensive material to a new/unique set of property/performance/price speci cations through the combinations of low-cost or high-performance materials. Various miscible or partially miscible blends based on Hoechst Celanese PBI and commercially available polyimides (PI), polyamideimide (PAI), poly(4-vinyl pyridine) (PVPy), polyarylate (PAr), and high-modulus aramide (HMA) have been discovered [19–41]. Blend

Downloaded by [Yan Wang] at 17:51 05 January 2016

© 2016 by Taylor & Francis Group, LLC

miscibility was evidenced in the form of infrared (IR) spectra, single T_g values, and well-de ned single tan δ relaxations. The intermolecular interactions involving the >NH and carbonyl groups are the major driving forces for the miscibility. Immiscible blends such as PBI and polysulfone (PSF) were also reported [41–43]. Lithium chloride (LiCl) plays an important role on dope stability and process window of these miscible and nonmiscible blends.

Model and Lee [44,45] and Model et al. [46] investigated the uniqueness of PBI at membranes, hollow bers, as well as fabrication process, whereas Hughes et al. [47] summarized the overall processes, from PBI powder formation, cold molding, sintering, to their performance. Brooks et al. [48] reported the water absorption phenomenon of PBI materials.

19.2 SYNTHESIS

19.2.1 General Route

In fact, Brinker and Robinson [49] were the rst inventors of aliphatic PBIs, whereas Vogel and Marvel [1,50] modi ed their approach and synthesized the rst aromatic PBIs. Since then, many methods for synthesizing PBIs have been invented [2–8]. Experimental data indicate that aromatic PBIs have thermal properties that are remarkably better than their aliphatic ones, as illustrated by Table 19.1 for several types of PBIs [3,5].

The general route to synthesize PBIs from aromatic tetraamines (bis-*o*-diamines) and dicarboxylates is illustrated in Figure 19.1 [5]. Generalized monomers are shown on the left-hand side, whereas the resultant PBIs are on the right-hand side. R_1 and R_2 are either aromatic or aliphatic and could contain other groups, such as ether, ketone, sulfone, etc. The phenyl groups shown in Figure 19.1 could be replaced by naphthyl groups. Polymerization could take place in either melt or solution.

19.2.2 Specific Case for PBI

Poly[2,2′-(*m*-phenylene)-5,5′-bibenzimidazole] is the dominant commercially available PBI and has received the most attention. Two approaches have been developed to synthesize this polymer: one is a conventional two-stage reaction, and the other is a single-stage reaction. Figure 19.2 illustrates

TABLE 19.1
Structure and Stability of Several Polybenzimidazoles

Tetraamine	Acid	MP(°C)	Weight Loss (%) in N_2	Weight Loss in Air (%)[a]
	3,4-Diaminobenzoic	>600	0.4	–
Biphenyl	Terephthalic	>600	0	–
Benzene	Terephthalic	>600	1.0	–
Biphenyl	Isophthalic	>600	0.4	5.2
Benzene	Isophthalic	>600	0.3	–
Diphenylether	Isophthalic	>400	–	–
Biphenyl	Phthalic	>500	0.4	7.0
Biphenyl	4,4′-Oxydibenzoic	>400	–	–
Biphenyl	Biphenyl-4,4′ diacid	>600	0.8	–
Biphenyl	Biphenyl-2,2′ diacid	>430	8.0	–

Source: A. H. Frazer, *Polymer Reviews*, vol. 17, Interscience, New York, 1968, p. 138; Reprinted from *High Performance Polymers*: *Their Origin and Development* (R. B. Seymour and G. S. Kirshenbaum, eds.), E. D. Powers, and G. A. Serad, History and development polybenzimidazoles, 355, Copyright 1986, with permission from Elsevier.

[a] Weight loss after 1 h at 500°C, and after 1 h at 400°C and 450°C.

Downloaded by [Yan Wang] at 17:51 05 January 2016

© 2016 by Taylor & Francis Group, LLC

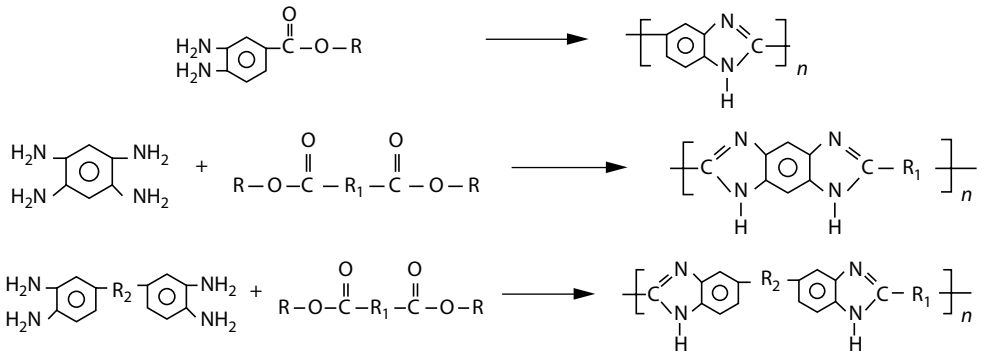

FIGURE 19.1 Polybenzimidazoles synthesized from different monomers. (Reprinted from *High Performance Polymers*: *Their Origin and Development* (R. B. Seymour and G. S. Kirshenbaum, eds.), E. D. Powers, and G. A. Serad, History and development polybenzimidazoles, p. 355, Copyright 1986, with permission from Elsevier.)

Downloaded by [Yan Wang] at 17:51 05 January 2016

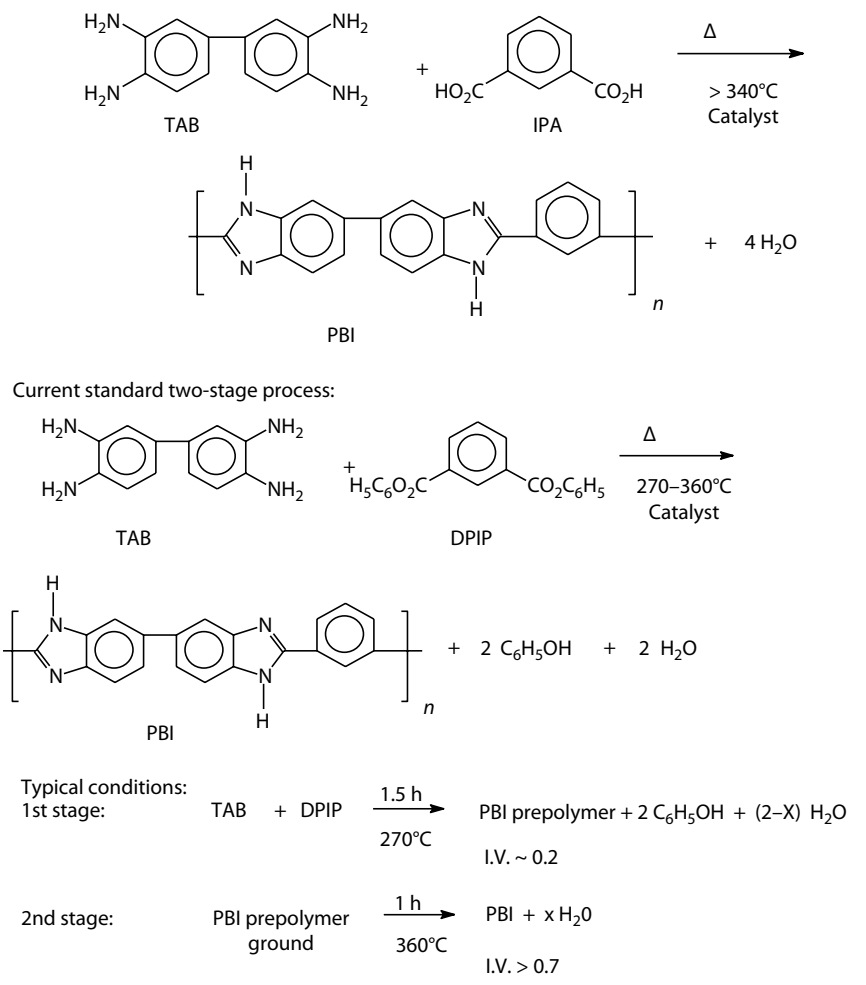

FIGURE 19.2 Two routes to synthesize PBI. (E. W. Choe: Catalysts for the preparation of polybenzimidazoles. *J. Appl. Polym. Sci*. 1994. 53. 497. Copyright Wiley-VCH Verlag GmbH & Co. KGaA. Reproduced with permission.)

© 2016 by Taylor & Francis Group, LLC

TABLE 19.2
Major Differences between Single-Stage and Two-Stage Polymerizations

	Single-Stage Polymerization	Two-Stage Polymerization
Major Monomers	**TAB and Isophthalic Acid (IPA)**	**TAB and Diphenylisophthalate (DPIP)**
Reaction temperature and time	400°C for 1 h	1st stage: 270°C for 1.5 h 2nd stage: 360°C for 1.0 h
By-products	Water	Phenol and water
Antifoaming agent	No	Yes
Catalysts	Needed	Optional
Cost	Medium	High

Source: E. W. Choe, *J. Appl. Polym. Sci.* 53: 497, 1994.

TABLE 19.3
Preferred Monomer Suppliers and Properties

	TAB	DPIP	IPA
Producer	Hoechst	Amoco	Burdick and Jackson
Purity (%)	96.7	99.9+	99.5
Melting point (°C)	177.0	339	136

Source: E. W. Choe, *J. Appl. Polym. Sci.* 53: 497, 1994.

the details of these two reaction schemes [10]. The major differences between these two approaches are summarized in Table 19.2.

Polymerization of this PBI takes place in either melt or solution. The reaction kinetics and mechanisms are well known [5,6], and there is no need to repeat them here. However, it is important to point out that polymerization should take place under anaerobic conditions due to the fact that aromatic amines tend to form oxides. PBI made under nitrogen environment seems to have a better quality (less gel) than that made in vacuum [5,6,10]. In the case of a two-stage polymerization scheme, a voluminous foam is created owing to the entrainment of gaseous by-products. This foam can be signi cantly reduced by increasing the internal pressure of the reactor to 2.1–4.2 MPa (300–600 psi) or by adding an antifoaming agent. Foaming is not a severe phenomenon in the single-stage polymerization.

Buckley et al. [6] described the speci cations of monomers for PBI polymerization. In short, extreme purity is required. Table 19.3 lists the monomer suppliers and properties used by Choe [10]. Triaminobiphenyl (≈2.9%) and other extraneous impurities (0.2%) are major impurities in 3,3′,4,4′-tetraaminobiphenyl (TAB). The former may slightly in uence chain growth during polymerization, whereas the latter may induce branching and gelation [6]. These impurities must be reduced to trace amounts if possible.

19.2.3 Product Requirements and Catalyst Effects

19.2.3.1 Requirements

Before discussing the effects of catalysts on PBI resins, we need to de ne the required quality for a ber-grade PBI. Generally, a synthesized PBI is useful for ber spinning if it meets the following three criteria [5,6,10,51]:

Downloaded by [Yan Wang] at 17:51 05 January 2016

© 2016 by Taylor & Francis Group, LLC

1. Inherent viscosity (IV) is between 0.7 and 0.75 dL g^{-1}.
2. The plugging value is greater than 0.5 g/cm^2.
3. The insoluble matter is less than 1%.

IV is measured in a concentration of 0.4% PBI in 100 mL of 97% sulfuric acid. Since IV is a simple but indirect measurement of molecular weight, a polymer with a reasonably high IV usually yields a ber with better mechanical properties. The plugging value is de ned as the theoretical weight in grams of polymer that would pass through 1 cm^2 of a lter in in nite time in order to plug it. This is a measurement of solution lterability and is obtained by plotting the weight of polymer, which passes through a sheet of Gelman type A glass paper (Gelman Science Inc., Ann Arbor, MI) under 1 atm pressure versus time before becoming blocked. The bigger the plugging value, the better the solution lterability. The PBI concentration normally used in this measurement is about 5–7% in 97.0 ± 0.1% sulfuric acid. A detailed technique for measuring the plugging value appears elsewhere [6,10,51]. The insoluble matter is measured in *N,N*-dimethylacetamide (DMAc) solution containing 2% LiCl. The insoluble materials may result from the impurities of the monomers.

Downloaded by [Yan Wang] at 17:51 05 January 2016

19.2.3.2 Catalyst Effects

19.2.3.2.1 Single-Stage Reaction

Choe [10] brie y reviewed previous work on the effects of catalysts on various PBIs [52–59] and conducted an extensive study on PBI syntheses. More than 15 catalysts were used to investigate the effects of a catalyst's chemistry on PBI's IV and plugging value. The following are considered to be good catalysts because they produce PBIs with an IV greater than 0.7 dL g^{-1}, a plugging value greater than 0.5, and an insoluble matter in DMAc less than 1%: dichlorophenylphosphine, chlorodiphenylphosphine, triphenyl phosphite, diphenylphosphine oxide, diphenylchlorophosphate, triphenyl phosphate, dimethoxyphenylphosphine, dibutoxyphenylphosphine, *o*-phenylphosphorochloridite, phenyl *N*-phenylphosphoramidochloridate, and dichlorodimethylsilane.

Choe [10] also reported the effects of catalyst concentration on PBI polymerization and showed that IV increases with an increase in catalyst concentration reaching almost a plateau at 1% concentration. Polymerization temperature also plays an important role on PBI properties. If 1% dichlorophenylphosphine ($C_6H_5PCl_2$) is used as the catalyst, a temperature of 390°C is required to yield a satisfactory product. A temperature of 400°C would be needed if one were to use 1% triphenyl phosphite $(C_6H_5O)_3P$ as the catalyst.

19.2.3.2.2 Two-Stage Reaction

Choe's data suggest that phosphorus-containing catalysts usually produce satisfactory products in the two-stage polymerization of PBI resins. Buckley et al. [6] had described the detailed process conditions and reactor vessels (sizes and reactor materials) for the two-stage polymerization reaction.

19.3 PBI FIBER FORMATION

19.3.1 Dope Preparation

Principally, PBI bers can be prepared through dry-spinning, wet-spinning, and dry-jet wet-spinning processes, but dry spinning is the preferred method. A few solvents, such as sulfuric acid, dimethylformamide, dimethylsulfoxide, and DMAc, would dissolve PBI, but DMAc is preferred for dry-spinning PBI bers [5,6,10,51,60]. Usually, spinning dopes contain 25–26 wt% of PBI and have a viscosity around 2000–3000 poise measured at room temperature. In order to prevent dopes from gelling or phasing out, 1–5 wt% LiCl or zinc chloride ($ZnCl_2$) (based on the weight of DMAc) is added to the spinning dopes. LiCl is preferred because it can be leached out easily during the subsequent washing stage. Table 19.4 summarizes the typical properties of PBI and sulfonated PBI bers [61].

© 2016 by Taylor & Francis Group, LLC

TABLE 19.4
Properties of PBI and Sulfonated PBI Fibers

Properties	Unstabilized PBI	Stabilized PBI
Denier per lament (dpf)	1.5	1.5
Tenacity (g/d)	3.1	2.7
Modulus (g/d)	90	45
Break elongation (%)	90	30

Source: Reprinted from *High Performance Polymers*: *Their Origin and Development* (R. B. Seymour and G. S. Kirshenbaum, eds.), E. D. Powers, and G. A. Serad, History and development polybenzimidazoles, 355, Copyright 1986, with permission from Elsevier; A. Buckley, D. Stuetz, and G. A. Serad: Polybenzimidazoles. *Encyclopedia of Polymer Science and Engineering* (J. I. Kroschwitz, ed.). 572. 1987. Copyright Wiley-VCH Verlag GmbH & Co. KGaA. Reproduced with permission; A. B. Conciatori et al., *J. Appl. Polym. Sci.* 19: 49, 1967; Hoechst Celanese PBI brochure, P.O. Box 32414, Charlotte, NC 28232-9973.

Note: Data obtained from the PBI brochure. g/d × 8.83 = cN/tex.

Downloaded by [Yan Wang] at 17:51 05 January 2016

19.3.2 Dry-Spinning Process

The dry-spinning process consists of three elements: a spinneret set, a circulated dry column, and a take-up unit. A spinneret may have 50–1000 holes with a diameter of about 75–100 μm. The take-up speed varies from 150 to 500 m/min. The dope is ltered and metered by a gear pump to the spinneret at 70–110°C, and the jet face temperature is about 100–150°C. Fiber is formed when most of the DMAc is vaporized. Generally, this is carried out during spinning by the circulating N_2 in a dry column, which is about 6.6 m long at a temperature of about 200–220°C, as illustrated in Figure 19.3. The residual DMAc in the as-spun ber is removed by washing with water. The as-spun ber property is weak; its tenacity is about 0.11–15 N/tex (1.3–1.7 g/day), modulus about 2.6–4.4 N/tex (30–50 g/day), and elongation at break of about 100–120%.

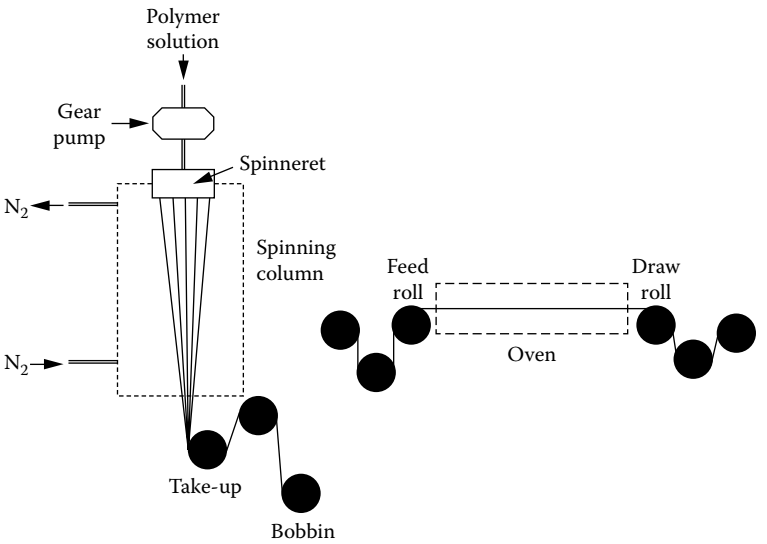

FIGURE 19.3 Typical drying-spinning and hot-draw devices.

© 2016 by Taylor & Francis Group, LLC

19.3.3 Hot Drawing

In order to improve ber properties, the as-spun ber could be hot-drawn by passing the dried la-ments through a heat muf e furnace at approximately 400–440°C dependent on the speed. Skewed rolls before and after the muf e furnace accurately maintain the laments at different speeds, as illustrated in Figure 19.3. The spin-line tension causes the laments to elongate and the polymeric structure within the bers become possibly better organized.

When the draw ratio varies from 1 to 4, the initial modulus may increase from 3.3 to 11 N/tex (from 36 to 122 g/day), whereas elongation at break may drop from 110% to 18%.

19.3.4 Sulfonation and Stabilization

In order to prevent PBI fabrics from shrinkage during burning, the drawn PBI yarn is acid-treated and stabilized to form a salt with the imidazole ring structure [5,6,10,51]. Sulfonation is conducted by dipping a hot-drawn PBI yarn in a 2% sulfuric acid bath for 2 h at 50°C. Stabilization of a sulfuric acid-treated ber is carried out by again passing it through a heat muf e furnace of approximately 380–440°C depending on the process speed. The ame shrinkage of a PBI ber is reduced from >50% to <10% after treatment.

19.4 PBI BLEND FIBERS

Although PBI has good mechanical properties, it is dif cult to be fabricated into large parts because of its high glass transition temperature (T_g ~425–435°C). Its moisture regain is high, and its thermo-oxidative stability at temperatures above approximately 260°C is not as good as that of some high-performance PIs. Blending may overcome the above shortcomings and extend its application range into the area of functional polymers. Luckily, PBI possesses both donor and acceptor hydrogen-bonding sites, which are capable of participating in speci c interactions and thus favorable to form miscible blends with some other polymers [9].

19.4.1 PBI/PI Blends

PBI/PI blends have received most attention because the blends synergize their strengths and overcome their individual shortcomings [27–31,62–66]. A research team was formed in the early 1980s to overcome the weaknesses of PBI through blending with a variety of PIs and to fundamentally understand the phase nature of the blends. This multisector research team includes the University of Massachusetts, Virginia Polytechnic and State University, Lockheed Aeronautical Systems, General Electric Aircraft Engine Business Group, and Hoechst Celanese. They report that PBI was miscible with a broad range of PIs, including ether imides, uoro-containing imides, and others [9,19–31,64–66]. Two blends were chosen as examples in this review. They were the 85:15 blend of PBI/PEI and the 10:90 PBI blend with a copolyimide containing 37.5 mol% of 4,4′-hexa uoroisopropylidenediphthalic anhydride (6FDA). The PEI used in this study was Ultem 1000 produced by General Electric. Table 19.5 illustrates the glass transition temperatures and other key parameters of the blend components. PBI has outstanding compressive properties that are essentially rendered onto the blends as illustrated in Tables 19.5 and 19.6 [9]. In addition, PBI/PEI and PBI/6FCoPI (i.e., 6FDA-polyimide) blends have better chemical resistance. For example, both PEI and 6FCoPI are attacked and softened by common solvents such as methylene chloride and acetone, whereas PBI and the two blends appear to be insoluble, even after 2-year exposure as thin lms. Mechanical properties of PBI/GFCoPI blends are listed in Table 19.7.

Although PBI/PI blends show a single T_g over the entire composition range on a rst heating by dynamic mechanical analysis (DMA), this single phase is metastable over much of the

Downloaded by [Yan Wang] at 17:51 05 January 2016

© 2016 by Taylor & Francis Group, LLC

TABLE 19.5
Structure and Properties of Candidate High-Temperature Matrix Polymers

Properties	PBI	PEI	6FCoPI
T_g (°C)	420	220	340
Tensile Properties			
Strength (MPa)	100	108	97.2
Elongation (%)	1.8	33	4.4
Modulus (GPa)	5.68	3.18	3.36
Flexural Properties			
Strength (MPa)	100	143	153
Modulus (GPa)	6.32	3.39	3.83
Compressive Properties			
Strength (MPa)	397	150	183
Modulus (GPa)	6.46	3.3	3.71

Source: M. Jaffe et al., *Adv. Polym. Sci.* 117: 297, 1994.

TABLE 19.6
Mechanical Properties of 85:15 PBI/PEI Blends

Tensile Properties	
Strength (MPa)	158
Elongation (%)	3.4
Modulus (GPa)	5.34
Flexural Properties	
Strength (MPa)	248
Modulus (GPa)	5.73
Compressive Properties	
Strength (MPa)	300
Modulus (GPa)	5.18

Source: M. Jaffe et al., *Adv. Polym. Sci.* 117: 297, 1994.

composition range in most cases [9,19–22,25,65]. Fourier transform IR spectroscopy (FTIR) data indicate that the origin of the miscible behavior in this system is a strong hydrogen bond interaction between the imidazole hydrogen and the carbonyl of the PI. Experimental data indicate that during the long annealing times above T_g often associated with the molding cycles for these materials, the carbonyl IR absorbance shift induced by the hydrogen bonding disappears. This indicates that phase separation has taken place in the blend, con rming the metastable nature of the observed miscibility.

Figure 19.4 illustrates the weight loss of the 85:15 PBI/PEI blend as a function of time during exposure in air at 315°C [9]. The rate of degradation is faster than that of either PBI or PEI. This is probably due to the fact that PBI accelerates the degradation of the PEI. In other words, the overall rate of degradation is exacerbated by the strong intimate interaction present within the blend.

Downloaded by [Yan Wang] at 17:51 05 January 2016

© 2016 by Taylor & Francis Group, LLC

TABLE 19.7
Mechanical Properties of 10:90 PBI/6FCoPI Blends

Tensile Properties	
Strength (MPa)	103
Elongation (%)	4.8
Modulus (GPa)	3.36
Flexural Properties	
Strength (MPa)	156
Modulus (GPa)	3.90
Compressive Properties	
Strength (MPa)	187
Modulus (GPa)	3.81

Source: M. Jaffe et al., *Adv. Polym. Sci.* 117: 297, 1994.

Downloaded by [Yan Wang] at 17:51 05 January 2016

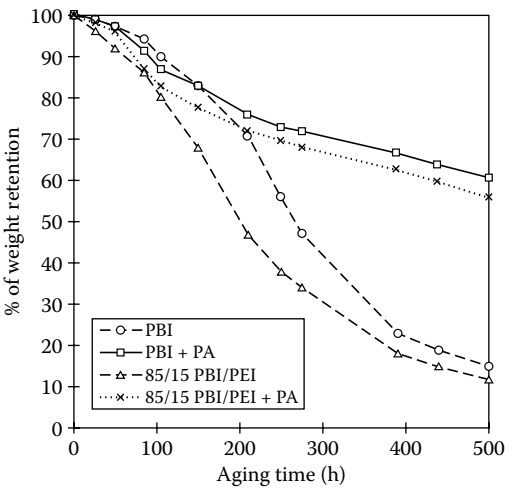

FIGURE 19.4 Effect of PA treatment on the thermooxidative stability of PBI and PBI/PEI blend lms aging at 315°C. (With kind permission from Springer Science+Business Media: *Adv. Polym. Sci.* High performance polymer blends, 117, 1994, 297, M. Jaffe, P. Chen, E. W. Choe, T. S. Chung, and S. Makhija.)

Protonation of the imidazole ring by phosphoric acid (PA) improves the thermooxidative stability of PBI, as well as the blend.

Figure 19.5 illustrates the weight loss of the 10:90 PBI/6FCoPI blend as a function of time during exposure in air at 315°C. The rate of degradation of PBI is signi cantly reduced by the addition of 6FCoPL. These excellent thermal properties indicate that the 10:90 PBI/6FCoPI is a matrix candidate for use at temperatures up to 315°C.

A series of asymmetric hollow ber membranes spun from PBI/PI blend solutions have been developed by Chung's group at the National University of Singapore recently [27,29,30,62,63]. Consistent with the aforementioned studies, the miscibility and molecular interactions between PBI and PEI were con rmed by various characterizations. An increase in PBI percentage in the spinning solutions could result in membranes with a tighter morphology, lesser nger-like voids, and signi cantly lower gas permeance. However, the gas separation [62] and pervaporation [27] performance of the resultant membranes were signi cantly improved.

© 2016 by Taylor & Francis Group, LLC

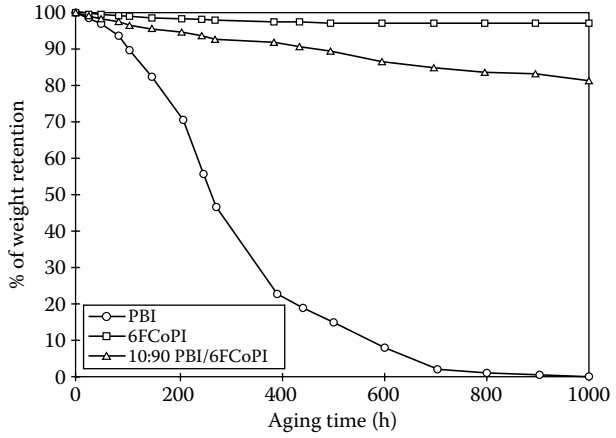

FIGURE 19.5 Thermooxidative stability of PBI and 6FCoPI blend films aged in air at 315°C. (With kind permission from Springer Science+Business Media: *Adv. Polym. Sci.* High performance polymer blends, 117, 1994, 297, M. Jaffe, P. Chen, E. W. Choe, T. S. Chung, and S. Makhija.)

Downloaded by [Yan Wang] at 17:51 05 January 2016

19.4.2 PBI/PAr Blends

PAr is a group of wholly aromatic polyesters derived from aromatic dicarboxylic acids and diphenols or their derivatives. They are amorphous in nature with a much lower cost than that of PBL. PAr and PBI have many common polar organic solvents (e.g., 1-methyl-2-pyrrolidinone [NMP], DMAc, dimethylsulfoxide [DMSO], etc.). NMP solutions containing 10 wt% of PBI and PAr were usually homogeneous and had no insolubles. After being kept at room temperature for a number of days, PBI-rich dopes precipitate, but these phased-out solids could be easily redissolved with a mild heating (e.g., 100°C for 20 min). Based on the haze level, the stability of the PBI/PAr/NMP increases with an increase in the relative PAr concentrations [33,34,36].

Figure 19.6 illustrates that the IV of the solution blends exceeds the rule of mixtures at a concentration of 0.5%. This result suggests that PBI and PAr exhibit strong interactions in a dilute solution such that the resulting hydrodynamic size of the blends is greater than the calculated averages based on each component. Corroborating evidence of a PBI–PAr interaction was observed by FTIR. Based on the carbonyl stretching of a pure PAr film, it was found that the signal of an 80:20 PBI/PAr film showed a dramatic downfield shift (i.e., from 1741 to 1730 cm^{-1}).

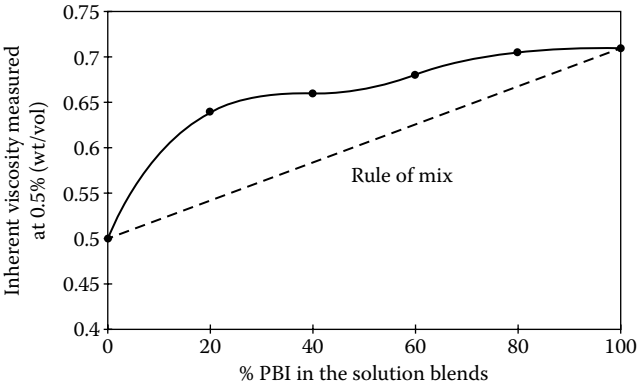

FIGURE 19.6 Relationship between the PBI/PAr blend IVs and compositions. (From T. S. Chung and P. N. Chen, Sr., *J. Appl. Polym. Sci.* 40: 1209, 1990; T. S. Chung and P. N. Chen Sr., *Polym. Eng. Sci.* 30: 1, 1990.)

© 2016 by Taylor & Francis Group, LLC

This shift (see Figure 19.7) indicates the existence of intermolecular H bonding between PBI and PAr in the lm blend. Similar to the case of PBI/PEI and PBI/6FCoPI, blending PAr with PBI improves the solvent resistance of PAr. For example, PAr is soluble in methylene chloride and tetrahydrofuran, whereas PBI is insoluble in these solvents. An 80:20 PAr/PBI lm kept its physical integrity after soaking in methylene chloride for 30 min, whereas a pure PAr lm would completely dissolve within 10 s.

Table 19.8 summarizes the as-spun ber tensile properties and illustrates the minimum LiCl effects on ber properties. These bers were further drawn at elevated temperatures at various draw ratios, and the drawn bers became stronger, as illustrated in Table 19.9. Drawing at 400°C at a ratio of 3.0 gave the best tensile modulus and strength. Table 19.10 provides a comparison of tensile properties among PBI/PAr, PBI/PSF, PBI/PEI, and PBI bers. This comparison was based on the highest modulus and tenacity of PBI/PAr, PBI/PSF, and PBI/PEI bers obtained from the previous literature. Dry-spun PBI/PAr has a very impressive tensile modulus and strength and can be suitable for engineering and aerospace applications. The thermal stability of PAr in the lm blends is dramatically improved with the presence of PBI, and the degree of improvement increased with the

Downloaded by [Yan Wang] at 17:51 05 January 2016

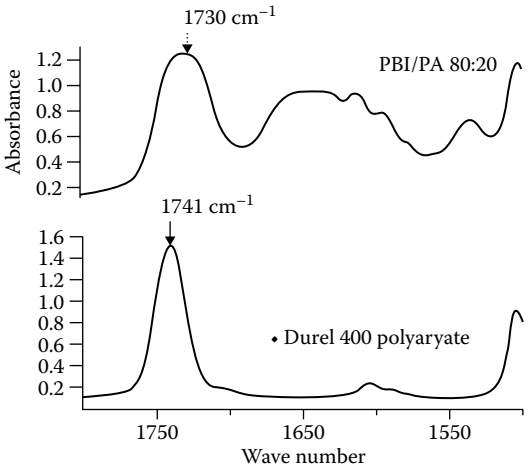

FIGURE 19.7 FTIR con rmation of the existence of intermolecular hydrogen bonding between PBI and PAr. (From T. S. Chung and P. N. Chen, Sr., *J. Appl. Polym. Sci.* 40: 1209, 1990; T. S. Chung and P. N. Chen Sr., *Polym. Eng. Sci.* 30: 1, 1990.)

TABLE 19.8
As-Spun 80:20 PBI/PAr and 80:20 PBI/PSF Fiber Properties

Sample	Spinning Method	Denier (dpf)	Initial Modulus (g/d)	Tenacity (g/d)	Elongation at Break (%)
80:20 PBI/PAr (LiCl)	Dry-spun	3.690	48.4	1.38	73.9
80:20 PBI/PAr (no LiCl)	Dry-spun	5.271	42.6	1.53	87.3
80:20 PBI/PSF	Wet-spun	30	30.2	0.97	4.0
80:20 PBI/PSF (LiCl)	Dry-spun	4.46	43.5	1.417	82.5
80:20 PBI/PSF (no LiCl)	Dry-spun	5.818	32.2	1.374	106.0

Note: g/d × 8.83 = cN/tex.

© 2016 by Taylor & Francis Group, LLC

TABLE 19.9
Properties of (80:20) PBI/PAr Fibers (No LiCl)

Draw Ratio	Temp. (°C)	Denier (dpf)	Initial Modulus (g/d)	Tenacity (g/d)	Elongation at Break (%)
2	400	1.919	77.69	3.118	29.50
2.5	400	1.915	91.86	3.313	17.92
3.0	400	1.501	141.15	4.611	6.75
2	420	1.668	66.50	2.922	33.75
3	420	1.453	80.74	3.378	19.75
4	420	0.951	113.86	4.014	11.61

Note: g/d × 8.83 = cN/tex.

TABLE 19.10
Property Comparison among Hot-Drawn PBI/PSF, PBI/PAr, PBI/Ultem, and PBI Fibers

Sample	Denier (dpf)	Draw Ratio	Initial Modulus (g/d)	Tenacity (g/d)	Elongation at Break (%)
PBI (LiCl)	1.7	2.0 at 440°C	91.0	4.0	31.9
PBI (no LiCl)	1.24	2.0 at 440°C	87.0	4.0	29.7
80:20 PBI/PAr (no LiCl)	1.501	3.0 at 400°C	141.15	4.611	6.75
80:20 PBI/PSF wet-spun (LiCl)	796	3.5 at 400°C	110.9	2.8	3.08
80:20 PBI/PSF (LiCl)	1.98	4.0 at 420°C	112.1	3.6	7.3
80:20 PBI/PSF (no LiCl)	1.00	4.5 at 420°C	134.1	4.84	5.9
75:25 PBI/Ultem	0.96	3.0 at 420°C	112.0	4.32	9.9

Note: g/d × 8.83 = cN/tex.

Downloaded by [Yan Wang] at 17:51 05 January 2016

increase in the PBI concentration (see Figure 19.8). Using the weight loss at 550°C as the reference, it is interesting to notice that the thermal stability of the blends was almost linearly proportional to the relative concentration of PBI (see Figure 19.9).

Table 19.11 summarizes the mechanical properties of hot-drawn and then acid-treated/stabilized bers. Both initial modulus and tenacity dropped due to the post-treatment, whereas their elongation

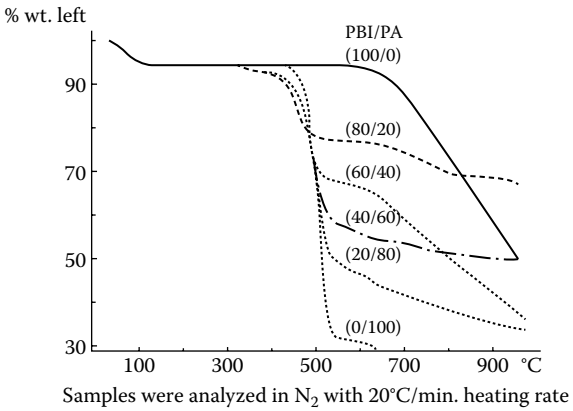

FIGURE 19.8 TGA study of PBI/PAr lm blends. (From T. S. Chung and P. N. Chen, Sr., *J. Appl. Polym. Sci.* 40: 1209, 1990; T. S. Chung and P. N. Chen Sr., *Polym. Eng. Sci.* 30: 1, 1990.)

© 2016 by Taylor & Francis Group, LLC

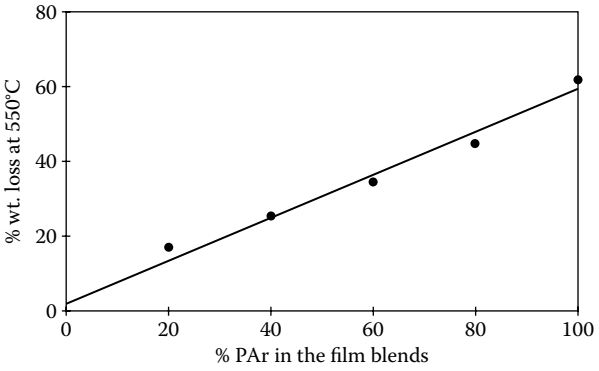

FIGURE 19.9 Correction between weight loss and PBI concentration in PBI/PAr films at 550°C. (From T. S. Chung and P. N. Chen, Sr., *J. Appl. Polym. Sci.* 40: 1209, 1990; T. S. Chung and P. N. Chen Sr., *Polym. Eng. Sci.* 30: 1, 1990.)

Downloaded by [Yan Wang] at 17:51 05 January 2016

TABLE 19.11
Tensile Properties of Sulfonated and Stabilized PBI, PBI/PAr, and PBI/PSF Fibers

Sample	Denier (dpf)	Initial Modulus (g/d)	Tenacity (g/d)	Elongation at Break (%)
PBI (LiCl)	1.5	45.0	2.7	30
80:20 PBI/PAr (no LiCl)	1.274	80.1	3.1	13.4
80:20 PBI/PSF (no LiCl)	2.526	58.7	2.6	19.1
80:20 PBI/PSF (LiCl)	1.337	71.5	2.24	5.9

Note: g/d × 8.83 = cN/tex.

increased. By hot-drawing an as-spun fiber 1–2 weeks after it had been spun, washed, and dried, the resultant fiber properties would drop significantly. Table 19.12 provides examples. This phenomenon is probably due to the effect of the vaporization of residual DMAc solvent on the phase stability of a compatible blend. Therefore, hot-drawing *immediately after* dry-spinning is the key to preparing high-modulus and high-tenacity fibers. Phase separation was evident in the transmission electron microscopy (TEM) micrographs (Figure 19.10) of an as-spun fiber (without LiCl), which was left at room temperature for 2 months. In contrast, the as-spun fibers with LiCl have a uniform texture with no evident phase separation as illustrated in Figure 19.11, and this structure is similar to the textures observed on the control PBI fibers. Figure 19.12 illustrates the FTIR spectra of 80:20 PBI/PAr films before and after the sulfonation and stabilization processes.

TABLE 19.12
Aging Effect on Tensile Properties of Hot-Drawn Fibers

Sample	Process Condition	Denier (dpf)	Initial Modulus (g/d)	Tenacity (g/d)	Elongation at Break (%)
80:20 PBI/PAr (no LiCl)	DIAS	1.501	141.1	4.6	6.75
80:20 PBI/PAr (no LiCl)	DL	1.600	101.2	3.7	7.01
80:20 PBI/PAr (LiCl)	DL	1.141	68.3	2.17	14.23
80:20 PBI/PSF (no LiCl)	DIAS	1.698	80.5	4.04	18.5
80:20 PBI/PSF (no LiCl)	DL	1.812	91.8	3.77	16.7

Note: g/d × 8.83 = cN/tex. DIAS: draw immediately after spun; DL: draw later.

© 2016 by Taylor & Francis Group, LLC

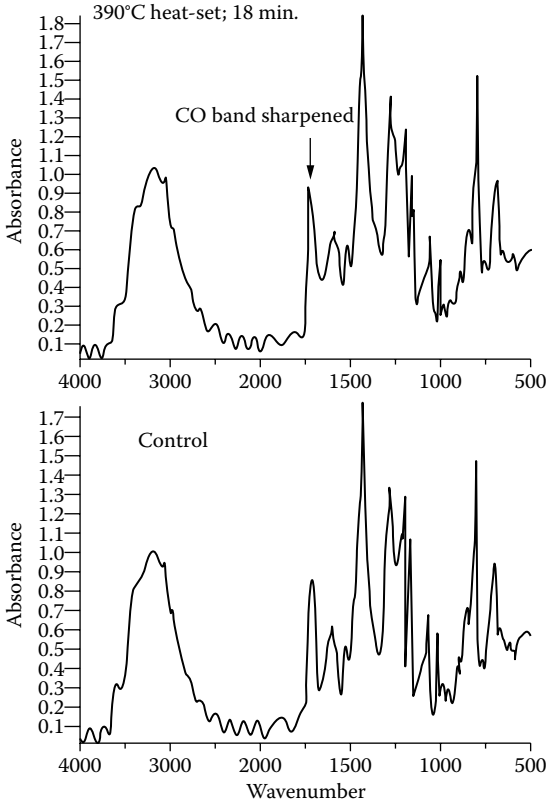

FIGURE 19.10 FTIR spectra for sulfonated 80:20 PBI/PAr (without LiCl) blends. (From T. S. Chung and P. N. Chen, Sr., *J. Appl. Polym. Sci.* 40: 1209, 1990; T. S. Chung and P. N. Chen Sr., *Polym. Eng. Sci.* 30: 1, 1990.)

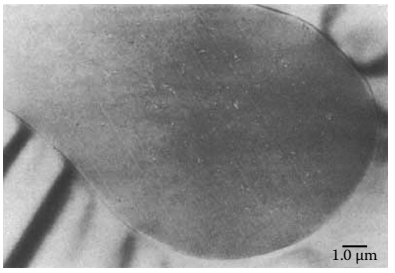

FIGURE 19.11 TEM micrographs of OsO_4 stained 80:20 PBI/PAr (without LiCl) blend fibers. (From T. S. Chung and P. N. Chen, Sr., *J. Appl. Polym. Sci.* 40: 1209, 1990; T. S. Chung and P. N. Chen Sr., *Polym. Eng. Sci.* 30: 1, 1990.)

19.4.3 PBI/HMA

Blending flexible coil polymers with rigid rod-like polymers has also generated interest. The resultant composites may have better fracture and impact toughness as well as thermal stability and flammability resistance. Two approaches of dispersing a rod-like polymer in a matrix were attempted. One involved synthesizing block copolymers, and the other involved blending solutions of two polymers. Takayanagi et al. [67] used the first approach to blend wholly aromatic polyamide such as poly(1,4-benzamide) (PBA), poly(1,4-phenyleneterephthalamide) (PPTA), and their block copolymers with nylon-6 or nylon-66. They found micro fibrils of PPTA dispersed in a fractured

Downloaded by [Yan Wang] at 17:51 05 January 2016

© 2016 by Taylor & Francis Group, LLC

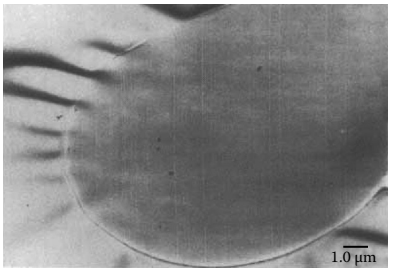

FIGURE 19.12 TEM micrographs of OsO_4 stained 80:20 PBI/PAr (with LiCl) blend bers. (From T. S. Chung and P. N. Chen, Sr., *J. Appl. Polym. Sci.* 40: 1209, 1990; T. S. Chung and P. N. Chen Sr., *Polym. Eng. Sci.* 30: 1, 1990.)

surface of the polymer composites. Wright–Patterson Air Force Laboratory was the driving force for the second approach and is also the leader for rod-like/random coil chain composites. They used very expensive materials, such as poly(*p*-phenylenebenzobisthiazole) (PBZT), as reinforcing elements [68–73]. Arnold and Arnold [73] reviewed on their work.

High-modulus polyaramides (HMAs) used here were synthesized from a low-temperature solution condensation reaction using terephthalic dichloride, *p*-phenylenediamine (25 mol%), 3,3′-dimethylbenzidine (37.5 mol%), and 1,4-bis-(4′-aminophenoxy)benzene (37.5 mol%) [35]. They have tensile properties similar to those of Teijin's HM-50 and DuPont's Kevlar. Figure 19.13 illustrates the TGA of neat polymers and their blends. The decomposition temperature of a 50:50 blend was in the range 400–450°C, i.e., higher than that of the neat HMA polymer, which demonstrated that PBI protected HMA from thermal degradation. The molecular interaction between the HMA and PBI was detected by observing the frequency of the amide–carbonyl band. In pure HMA, this band appeared at 1657 and was shifted to 1655 in an as-spun ber, to 1647 in a heat-treated and drawn ber [35]. The molecular interaction was found to be stronger on processing at a higher temperature as the bond energy of the carbonyl was weakest in this blend. The reduction in the carbonyl bond order would result from an interaction of the C=O with N–H. Figure 19.14 illustrates the TMA curves of HMA, PBI, and 50:50 HMA/PBI blend bers. For establishing miscibility in a blend system, one would expect a single tan δ peak intermediate in position to the two-component material peaks for a miscible blend system. This gure indicates that the 50:50 blend has a single tan δ at 380°C, which is between the peak of HMA (257.5°C) and PBI (425°C).

The 50:50 HMA/PBI blend bers were prepared from both dry-spun and wet-spun processes. The wet-spun ber properties were slightly inferior to those of dry-spun ones, as shown in Table 19.13.

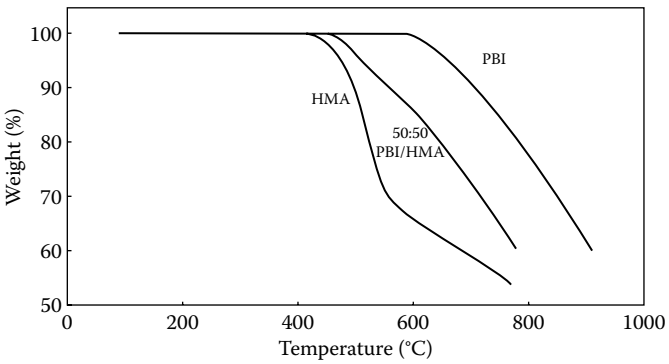

FIGURE 19.13 TGA curves of neat HMA, PBI, and 50:50 PBI/HMA. (From T. S. Chung and F. K. Herold, *Polym. Eng. Sci.* 31:1950, 1991; T. S. Chung et al., Fibers from blends of PBI with polyaramide and polyarylate, *Proceedings of Fiber Producer Conf.* (May) 1991, Greenville, SC. 3A-2.)

Downloaded by [Yan Wang] at 17:51 05 January 2016

© 2016 by Taylor & Francis Group, LLC

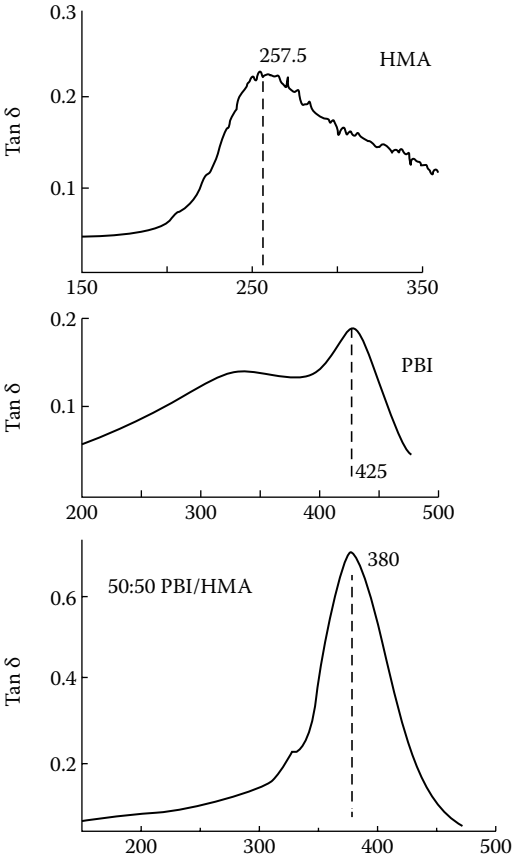

FIGURE 19.14 TMA curves of PBI, HMA, and 50:50 PBI/HMA bers. (From T. S. Chung and F. K. Herold, *Polym. Eng. Sci.* 31:1950, 1991; T. S. Chung et al., Fibers from blends of PBI with polyaramide and polyarylate, *Proceedings of Fiber Producer Conf.* (May) 1991, Greenville, SC. 3A-2.)

Downloaded by [Yan Wang] at 17:51 05 January 2016

TABLE 19.13
50:50 HMA/PBI Fiber Properties (Total Solid Content = 11% in DMAc)

Sample	Draw Ratio at 400°C	Denier (dpt)	Initial Modulus (g/d)	Tenacity (g/d)	Elongation at Break (%)
Wet-spun ber		9.8	73	1.78	23.46
Wet-spun and then hot-drawn	1.5	5.75	272	8.06	3.9
Wet-spun and then hot-drawn	2	4.54	269.8	6.93	3.12
Dry-spun ber		3.60	81.4	3.781	55.2
Dry-spun and then hot-drawn	2.5	1.406	252.1	9.65	10.38
Dry-spun and then hot-drawn	3.5	0.952	288.6	10.26	7.6
Dry-spun and then hot-drawn	4.5	0.783	302	10.83	7.3

Note: g/d × 8.83 = cN/tex.

© 2016 by Taylor & Francis Group, LLC

TABLE 19.14
20:80 HMA/PBI Fiber Properties (Total Solid Content = 17.8% in DMAc)

Sample	Draw Ratio at 400°C	Denier (dpf)	Initial Modulus (g/d)	Tenacity (g/d)	Elongation at Break (%)
			A: Wet-Spun		
As-spun		24.500	41.1	1.080	4.03
Hot-drawn	3	7.820	139.4	4.834	11.17
Hot-drawn	5	4.653	165.1	6.336	10.13
Hot-drawn	7	3.347	181.0	7.330	10.43
			B: Dry-Spun		
As-spun		4.933	49.96	1.740	80.48
Hot-drawn	2.5	2.021	137.91	5.031	18.44
Hot-drawn	3.5	1.554	170.64	6.400	10.87
Hot-drawn	4.5	1.121	184.76	5.710	6.47

Note: g/d × 8.83 = cN/tex.

Table 19.14 provides the tensile properties of dry-spun and wet-spun 20:80 HMA/PBI bers. The best conditions for obtaining a higher tensile modulus and strength for hot-drawing dry- and wet-spun bers were different. In the case of the wet-spun bers, the coagulation bath also had a signi cant effect on the ultimate ber properties. A mixture of ethylene glycol (EG)/DMAc solvent provided a better coagulation process and yielded a higher tensile modulus and strength ber than that of a water bath [35].

Similar to PBI/PAr blend bers, as-spun PBI/HMA bers seemed to become brittle after standing in the laboratory for a few weeks, probably due to the evaporation of residual DMAc solvent. Therefore, the hot-drawing process should take place immediately after dry spinning; otherwise ber properties will decay.

The mechanical properties of PBI/HMA blend bers follow the molecular composite theory developed by Halpin and Tsai [74]. The relationship of the composite modulus, E_{11}, to the individual moduli of the components is as follows:

$$E_{11}/E_m = (1 + \alpha b V_f)/(1 - b V_f) \tag{19.1}$$

where

$$b = (E_f/E_m - 1)/(E_f/E_m + \alpha) \tag{19.2}$$

where V_f is the volume fraction of ber, and E_t and E_m are the moduli of the ber and matrix, respectively. As the aspect ratio, α, becomes large, E_{11} approaches the limiting upper bound given by the following:

$$E_{11} = E_f V_f + E_m V_m \tag{19.3}$$

where V_m is the volume fraction of the matrix. This equation predicts that the composite modulus and tensile strength follow a linear *rule of mixtures* of the ber and matrix properties. Since the density of PBI is very close to that of HMA, the above can be further simpli ed as

$$E_{11} = E_f V_f + E_m V_m \tag{19.4}$$

where W is the weight fraction of the constituents, and subscripts f and m refer to ber and matrix, respectively. Figures 19.15 and 19.16 present the comparisons of the tensile modulus and strength of the hot-drawn bers obtained by experiments and predicted by the Halpin and Tsai equation

Downloaded by [Yan Wang] at 17:51 05 January 2016

© 2016 by Taylor & Francis Group, LLC

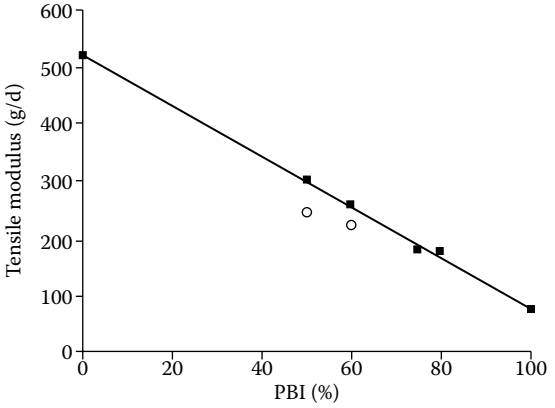

FIGURE 19.15 Tensile modulus of HMA/PBI as a function of PBI content. ■, Hot-drawn immediately after dry-spun; ○, drawn later. (From T. S. Chung and F. K. Herold, *Polym. Eng. Sci.* 31:1950, 1991; T. S. Chung et al., Fibers from blends of PBI with polyaramide and polyarylate, *Proceedings of Fiber Producer Conf.* (May) 1991, Greenville, SC. 3A-2.)

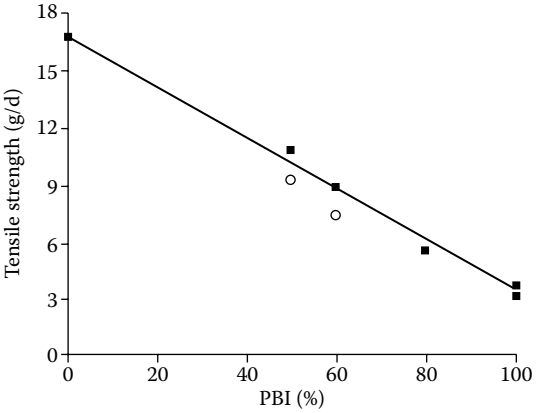

FIGURE 19.16 Tensile strength of HMA/PBI as a function PBI content. ■, Hot drawn immediately after dry-spun; ○, hot drawn later. (From T. S. Chung and F. K. Herold, *Polym. Eng. Sci.* 31:1950, 1991; T. S. Chung et al., Fibers from blends of PBI with polyaramide and polyarylate, *Proceedings of Fiber Producer Conf.* (May) 1991, Greenville, SC. 3A-2.)

Downloaded by [Yan Wang] at 17:51 05 January 2016

(straight lines). The agreement is good, and this implies that the PBI/HMA blend is miscible at the molecular level. However, the agreement becomes poor if the as-spun bers were aged and later hot-drawn, as illustrated in these two gures.

Recently, PBI/Kevlar (poly *p*-phenylene terephthalamide) blend staple bers were studied by Arrieta et al. [37,38] and Genc et al. [75] on their moisture sorption characteristics and thermal aging properties. The study showed that exposure to elevated temperatures (190–320°C) resulted in a rapid decrease in tensile breaking force retention for a fabric made of a 60:40 wt% blend of Kevlar and PBI bers [37]. X-ray diffraction, Raman, and differential thermal analyses (DTA) were carried out to evaluate the effect of thermal aging on the material's crystallinity and transition temperatures [38].

19.4.4 PBI/PSF Blends

PSF has a better hydrolytic stability than polyesters and polycarbonates. Its thermal stability is also very impressive. Thermal gravimetric analysis shows that Amoco's Udel P1700 is stable in air up

© 2016 by Taylor & Francis Group, LLC

to 450°C (840°F). Therefore, PBI/PSF blends were prepared to yield a low-cost, high-performance PBI variant.

Spinning dopes with different PBI/PSF ratios were prepared with a polymer concentration of 25.6 wt% and LiCl of 2 wt%. Preliminary ber properties indicate that the 80:20 PBI/PSF blend has the best tensile properties [41,42]. In addition, no phase separation was observed in the 80:20 PBI/PSF blend dope over a few months. Phase separation slowly occurred in the 60:40 PBI/PSF sample after a few weeks. The 20:80 PBI/PSF dopes phase-separate after a few days. Dopes were also prepared without the addition of LiCl. Their formulation was 27 wt% of 80:20 PBI/PSF in DMAc.

The presence of LiCl in a spinning dope plays an important role in determining the dope viscosity, process window, and ber properties. The addition of LiCl resulted in a lower dope viscosity due to some interaction among LiCl, PBI, and PSF [42]. As a consequence, the process windows for ber spinning are quite different for dopes with and without LiCl. Dopes without LiCl have a broad process window for ber spinning, and the resultant bers have superior properties.

Table 19.8 summarizes the as-spun PBI/PSF ber tensile properties and shows that LiCl has minimum effects on as-spun ber properties. LiCl effects appear on hot-drawn bers. Table 19.10 lists the best tensile modulus and strength of hot-drawn 80:20 PBI/PSF bers and compares them to those of PBI/PAr, PBI/Ultem, and PBI bers. Dry-spun 80:20 PBI/PSF bers (without LiCl) and PBI/PAr (without LiCl) have the best and almost the same tensile modulus and strength. Their properties are at least comparable to those of PBI/Ultem bers. Compared to standard PBI bers, these two blends have higher tensile moduli and strengths than those of PBI bers, whereas the elongations at break of the blends are inferior to those of the PBI.

FTIR spectra indicate a slight shift of the 1244 ether band of 4 cm^{-1} to lower frequency in the PBI/PSF blends, which would suggest a slight interaction between the NH and the O. The magnitude of this molecular interaction is very small compared to that for PBI/HMA (10 cm^{-1} wavelength shift) and for PBI/PAr (20 cm^{-1} wavelength shift). SEM pictures indicate that PBI/PSF blends are not miscible because they phase-separate.

The mechanical properties of acid-treated and stabilized 80:20 PBI/PSF bers are presented in Table 19.11. Both 80:20 PBI/PSF with and without LiCl bers have better moduli than that of stabilized PBI bers, whereas the PBI has the highest elongation at break. This is due to the fact that these PBI/PSF bers have been hot-drawn at high draw ratios. The 80:20 PBI/PSF ber with LiCl appeared to have PBI-like limiting oxygen indices (LOIs) and ame shrinkage behavior [41].

The PBI/PSF ber does not show aging phenomenon if hot-drawn later, as illustrated in Table 19.12. There is no major difference in properties for PBI/PSF bers drawn at different periods, whereas tensile modulus and strength properties drop signi cantly for PBI/PAr and PBI/HMA bers. This phenomenon is probably due to the effect of the vaporization of residual DMAc solvent on the phase stability of a compatible blend. As PBI/PSF blends are not compatible, the effect of DMAc on the phase stability is minor.

PBI/PSF blend hollow ber membranes were also wet-spun from highly concentrated immiscible blend solutions by Chung et al. [43]. A sharply de ned unit-step morphological change was found in the middle of the membrane cross section. A yellowish halo with a wavelength of 580–595 nm was observed, and its formation was possibly caused by a physical phenomenon, but not by the phase separation of PBI and PSF.

19.4.5 PBI/PAI Blends

Generally, PAIs are prepared by the condensation polymerization of a trifunctional acid anhydride (e.g., trimellitic anhydride [TMA]) with an aromatic diamine (e.g., 4,4′-methylene- or 4,4′-oxydianiline, i.e., MDA or ODA). These polymers are characterized by excellent high-temperature properties with T_g values typically above 270°C and continuous service temperatures of about 230°C. Since PAI has an imide structure on its polymer chains, hydrogen bonding could be formed between the carbonyl group of PAI's PI units and the NH group of PBI. PBI and Torlon 4000T were discovered

Downloaded by [Yan Wang] at 17:51 05 January 2016

© 2016 by Taylor & Francis Group, LLC

to be miscible at a molecular level over the whole composition range as con rmed by microscopy, differential scanning calorimeter (DSC), FTIR, and DMA [32]. FTIR spectra show the existence of hydrogen-bonding interactions in the polymer blends, whereas DSC and DMA studies con rmed the existence of a single glass transition in each blend.

19.4.6 PBI/PVPy Blends

Poly(2,2′-(*m*-phenylene)-5,5′-bibenzimidazole) is miscible with PVPy over the entire composition range [40]. Single T_g values, intermediate between the two pure polymers, were observed. FTIR data indicate that the –NH group of PBI forms a hydrogen bond with the N of PVPy. However, the thermal stability of these blends is not signi cantly high but similar to the thermal stability of pure PVPy.

19.5 MOLDED PBI PARTS

Three-dimensional PBI parts were developed from the melt-derived PBI powders by a hot compression molding (hcm) process in the 1980s [18,76,77]. The original process was very complicated and time consuming. For example, PBI powders were rst cold-pressed in a billet mold, and then the clamped mold was transferred to an oven for heating at a temperature above the T_g of PBI (425–435°C) for a period of 5–10 h. After cooling, the billet was cut and machined to the desired shape. This process was signi cantly simpli ed by Hughes et al. [47], who discovered that the use of porous PBI powders with reasonable moisture content was the key. In other words, porous PBI powders with reasonable moisture content could be cold-compacted at room temperature, while melt-derived PBI powders made directly from the solid state reactor (the second reaction in a two-stage PBI polymerization) could not. Figure 19.17 illustrates the morphology of melt-derived PBI powders and porous PBI powders. The porous PBI powders are prepared by spraying a 12 wt% PBI/DMAc solution into a water mist, as illustrated in Figure 19.18. The spraying nozzle is 100 μm with a pressure of 100 psi, and the PBI/DMAc dope viscosity is about 700 cp.

Two stages are needed for fabrication of PBI parts: cold-compact porous PBI powders, followed by their placement in a graphite powder bed under a pressure of 1–3 kpsi at 425–500°C for a few hours, as shown in Figure 19.19. This process is referred to as powder-assisted hot isostatic pressing (HIP) [47]. Table 19.15 summarizes the results and compares the mechanical properties of PBI parts made from the different approaches. Clearly, samples made from the new approach (df as de ned in the table) yield the best properties.

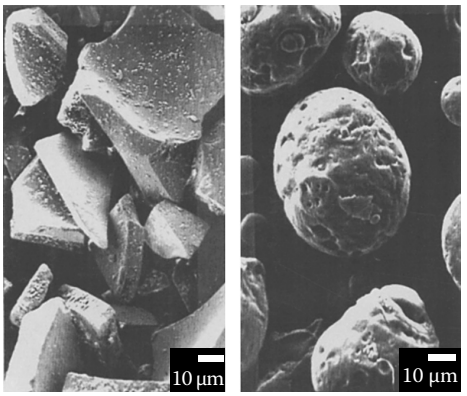

FIGURE 19.17 Morphology of melt-derived PBI powders (a) and spray precipitation porous PBI powders (b). (O. R. Hughes, P. N. Chen, W. M. Cooper, L. P. DiSano, E. Alvarez, and T. E. Andres: PBI powder processing to performance parts. *J. Appl. Polym. Sci.* 1994. 53. 485. Copyright Wiley-VCH Verlag GmbH & Co. KGaA. Reproduced with permission.)

Downloaded by [Yan Wang] at 17:51 05 January 2016

© 2016 by Taylor & Francis Group, LLC

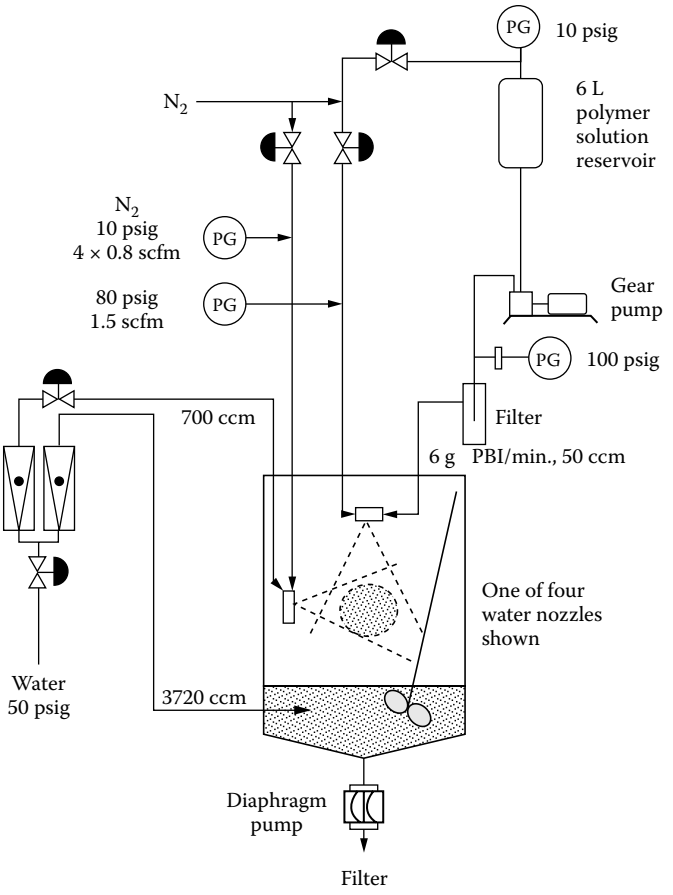

FIGURE 19.18 Schematic diagram of the spray precipitation reactor. (O. R. Hughes, P. N. Chen, W. M. Cooper, L. P. DiSano, E. Alvarez, and T. E. Andres: PBI powder processing to performance parts. *J. Appl. Polym. Sci.* 1994. 53. 485. Copyright Wiley-VCH Verlag GmbH & Co. KGaA. Reproduced with permission.)

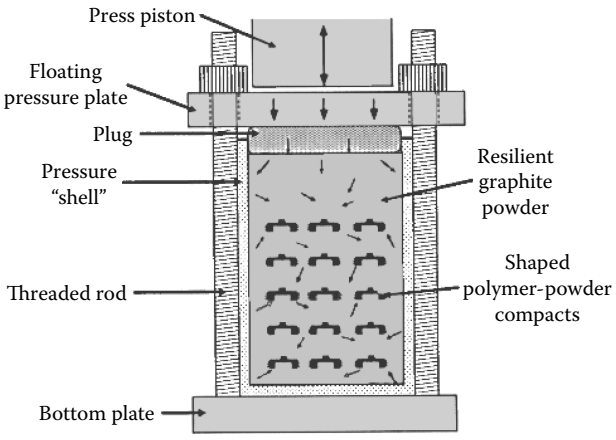

FIGURE 19.19 Pressure vessel and clamp assembly for powder-assisted HIP process. (O. R. Hughes, P. N. Chen, W. M. Cooper, L. P. DiSano, E. Alvarez, and T. E. Andres: PBI powder processing to performance parts. *J. Appl. Polym. Sci.* 1994. 53. 485. Copyright Wiley-VCH Verlag GmbH & Co. KGaA. Reproduced with permission.)

Downloaded by [Yan Wang] at 17:51 05 January 2016

© 2016 by Taylor & Francis Group, LLC

© 2016 by Taylor & Francis Group, LLC

Downloaded by [Yan Wang] at 17:51 05 January 2016

TABLE 19.15
Molded PBI Materials: Process Conditions and Properties

		Molding Conditions				Tensile Properties					
PBI Powder Type	**Filler**	**Process**	**Temp. (°C)**	**Press. (kpsi)**	**Time (h)**	**Density (g/cm^3)**	**Strength (kpsi)**	**Elong. (%)**	**Modulus (mpsi)**	**Compression Strength (kpsi)**	**Izod Impact Strength (Unnotched) (ft-lb/in.)**
Melt-derived	None	hcm	462	3.00	0.50	1.278	22.9	3.0	0.850	57	6.7
	None	hcm	463	3.00	4.00	1.276	27.1	3.8	0.830	–	9
Spray-precipitated	None	hcm	461	3.00	0.50	1.285	26.5	3.5	0.857	–	9.8
	None	hcm	460	2.00	2.00	1.280	27.8	3.7	0.870	60	–
	None	hcm	463	3.00	4.00	1.277	31.3	4.4	0.836	–	15.2
Spray-precipitated	None	df	463	1.00	4.00[a]	1.300	32	5.0	0.950	–	–

Note: hcm = Hot compression molded to panel shape, machined to nal test shape. df = direct formed: cold compacted and HIP'd to billet shape, machine to nal test shape.

[a] Approximate time and temperature; actual conditions vary with vessel size.

19.6 PBI MATRIX RESINS AND COMPOSITES

The use of PBI as a matrix resin for continuous ber composites has received a lot of attention since the 1960s and 1970s because of its high performance at elevated temperatures [78–83]. The amount of research in these areas has been gradually decreased because of (1) the availability of many high-performance polymers, such as polyetherketone (PEEK), liquid crystalline polymers (LCPs), PIs, and polyphenylene sul de (PPS) in the 1980s and 1990s, and (2) PBI's high water absorption characteristics. For example, PBI can absorb 15–18% water by weight, and this water may degrade the mechanical properties and bonding strengths of a PBI composite. Water absorption phenomenon of PBI was investigated by Brooks et al. [48], and molecular modeling of hydrated PBI was undertaken by Iwamoto [84].

PBI-based mixed-matrix bers with different nano llers are developed in recent years, including carbon bers [79], carbon nanotubes [80], polyhedral oligomeric silsesquioxane (POSS) nanoparticles [81], nano bers [82], and zeolitic imidazolate frameworks (ZIFs) [83]. It was reported that the incorporation of a small amount (0.5 wt%) of POSS nanoparticles into the PBI dope has signi cant in uence on both the morphology and the separation performance of the forward osmosis dual-layer hollow ber membranes [81]. The in-plane thermal conductivity of the carbon nanotube/PBI composites could be increased by a factor of 50 when incorporating 1.94 wt% carbon nanotubes into the composite nano bers [80]. Hollow ber membranes fabricated from the blend solution of PBI and synthesized nanoporous ZIF-8 nanoparticles for gas separation showed an impressive enhancement in H_2 permeability as high as a hundred times without any signi cant reduction in H_2/CO_2 selectivity [83]. The details are discussed in Section 19.9.5.

19.7 PBI APPLICATIONS IN HIGH-TEMPERATURE POLYMER ELECTROLYTE MEMBRANE FUEL CELLS

Through the evolution of technology and the rapid increase in global population, the demand for energy is ever increasing. According to the National Petroleum Council, the world's energy demand increased by approximately 50% over the last 25 years and is expected to do so again by 2030 [85]. Due to the ever-rising demand for energy and the nite resources available, it is no surprise that alternative energy sources and methods of clean energy production are needed. British Petroleum and Royal Dutch Shell, two of the world's largest oil companies, estimate that by 2050, one-third of the world's energy will need to be produced from alternative energy sources as a result of the growing population and the limited resources available [86]. A clean energy conversion device that has gained worldwide attention because of its potential use in stationary and mobile devices is the polymer electrolyte membrane (PEM) fuel cell, also known as the proton exchange membrane fuel cell [87]. Due to the excellent production of energy and the lack of harmful by-products, PEM fuel cells have received much attention as an alternative to combustion-based energy production [88]. PEM fuel cells produce energy at the heart of the cell, the membrane electrode assembly (MEA), which consists of a polymer matrix doped with electrolyte and sandwiched between two gas diffusion layers coated with metal catalyst. When fueled by hydrogen, the catalyst at the anode side splits the hydrogen into protons and electrons. The protons diffuse across the polymer membrane, and the electrons travel around the membrane through an external circuit. The protons and electrons react with the oxidant (typically oxygen or air) at the metal catalyst layer on the cathode side and produce water, thereby completing the electrochemical cycle. Hydrogen gas is the most commonly used fuel source for PEM fuel cells, although other fuel sources such as methanol, ethanol, and methane have been studied [89].

19.7.1 Low versus High Operational Temperature for PEM Fuel Cells

While PEM fuel cells have received much attention as promising energy conversion devices, limitations are associated with the availability and development of materials that would allow for the cost of manufacturing and production of these devices to compete with existing energy sources [88].

Downloaded by [Yan Wang] at 17:51 05 January 2016

© 2016 by Taylor & Francis Group, LLC

One possible way to overcome this limitation is to increase the ef ciency of these PEM fuel cells. By operating at elevated temperatures (>100°C), the ef ciency of the fuel cell is greatly increased and offers many advantages over lower operational temperatures [90]. PEM fuel cells that use low boiling point dopants such as water typically operate around 80°C to ensure that the electrolyte is not vaporized [89]. When water is used as the electrolyte, most commonly used with a per uorosulfonic acid membrane, additional components to prevent membrane dehydration are required. To ensure that heat generated by the cell does not vaporize the electrolyte, large heat exchangers are necessary. Another additional component is the dual-phase water system needed to regulate humidity [89]. If the humidity is too low, the membrane will dry out causing conductivity to dramatically decrease; however, if the humidity is too high, water condenses and the gas diffusion electrodes are ooded [89,91]. Under fully humidi ed conditions, a per uorosulfonic acid membrane (e.g., Na on) doped with water can reach a conductivity as high as 0.1 S cm^{-1} [91]. An additional problem associated with low operational temperatures is the poisoning of the catalyst from impurities in the fuel source, mainly carbon monoxide and hydrogen sul de [91]. The tolerance of the catalyst to impurities, which has been found to be temperature dependent, is much less problematic at elevated temperatures due to reversible binding of the impurity to the catalyst. Therefore, when operating at low temperatures, an extremely pure fuel source is required [89]. In order for a PEM fuel cell to operate at high temperatures (120–200°C), the electrolyte must have a high-enough boiling point to withstand operational temperature, and the polymer membrane must be thermally stable. Typically inorganic acids with low vapor pressures, such as PA and sulfuric acid, are used as electrolytes for high-temperature PEM fuel cells. There are many bene ts to operating at these increased temperatures. Since these polymers and electrolytes can withstand high temperatures, smaller heat exchangers can be used [89] and the fuel cells do not require a humidi cation process. As previously stated, the tolerance to gas impurities is greatly increased at these temperatures due to reversible binding. Not only is the catalyst less likely to be poisoned from the gas impurities, but also fuel sources with larger amounts of impurities can still be effectively used, thereby lowering reformation costs [89]. Additionally, operating at higher temperatures has been shown to increase the electrode kinetics, thus increasing performance and ef ciency overall.

Downloaded by [Yan Wang] at 17:51 05 January 2016

19.7.1.1 PBIs for High-Temperature PEM Fuel Cells

PBIs have attracted much attention as PEMs in high-temperature fuel cells due to their thermal and chemical resistances as well as their ability to form proton-conducting membranes. The basic sites along the PBI backbone allow for an acid–base complex to form with PA and sulfuric acid [90]. When doped with PA, this complex demonstrates high proton conductivity, low gas permeability, and a stable operational life of over two years. Though PBI doped with PA is conductive, it is important to note that PBI without an electrolyte has a negligible conductivity [90]. It is often bene cial to control the amount of PA dopant in the membrane. Excess PA can block oxygen diffusion into the catalyst layer, and insuf cient PA can lead to incomplete contact between the PBI/PA complex and the catalyst layer, thereby decreasing ef ciency [91]. PBIs imbibed with acid are promising candidates for low-cost, high-performance PEM materials and are readily producible [92].

19.7.1.2 Preparation of PBI–Acid Membranes

The morphology of a polymer membrane, which is greatly in uenced by polymer processing, can directly affect the properties of a PBI membrane. The method through which the PBI is imbibed impacts the amount of PA that can be contained within the membrane, thereby affecting conductivity. In the past, three preparation methods have been explored for imbibing PBI with PA.

19.7.1.2.1 Conventional Acid Imbibing

The conventional and most common method of doping PBI with PA consists of a multistep process, which is illustrated in Figure 19.20 [93,94]. The PBI is formed by two-stage melt/solid polymerization, and the powder form is dissolved in an organic solvent such as dimethylacetamide (DMAc)

© 2016 by Taylor & Francis Group, LLC

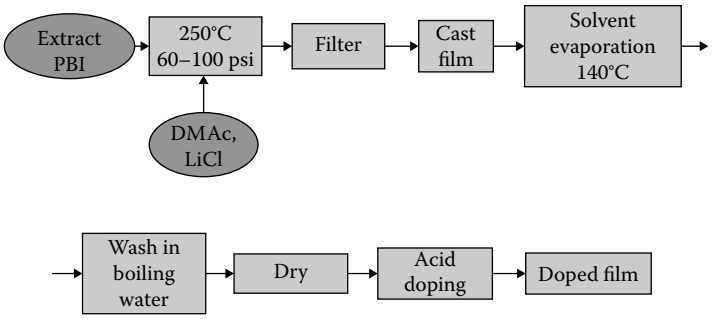

FIGURE 19.20 Step-by-step method of conventional PA imbibing of polybenzimidazole.

with LiCl for a stabilizer under pressure at 60–100 psi and at 250°C [89]. Any cross-linked PBI is removed by filtering, and the non-cross-linked polymer is then cast from solution and dried under vacuum to remove DMAc. The film is then washed in boiling distilled water to remove the LiCl and any remaining DMAc. Finally, the polymer is dried and placed in a PA bath for doping [89,92].

19.7.1.2.2 Porous PBI

In 2004, another method of imbibing PBI with PA was reported. In this method, a porous PBI film is created by casting a solution containing both PBI and a porogen (phthalates or phosphates) onto an untreated glass plate [95]. Once cast, the film is dried at 110°C for 2 h, and the porogen is removed by soaking the film in methanol. After drying a second time, the porous membrane is immersed in a concentrated PA solution for 4 days, and the membrane is blotted dry [95]. Figure 19.21 demonstrates the step-by-step process of synthesizing and imbibing the porous PBI membrane with PA.

19.7.1.2.3 Sol–Gel Process

The sol–gel process, also termed the polyphosphoric acid (PPA) process, was reported in 2005 by Xiao et al. [93]. Through this method, PBI is polymerized in PPA, which acts as both the polymerization solvent and the polycondensation reagent. Polymerization takes place at 190–220°C for 16–24 h and is then cast while hot directly onto untreated glass plates [93]. Once cast, the PPA is hydrolyzed under controlled conditions. Since both PBI and PPA are hygroscopic, moisture from the

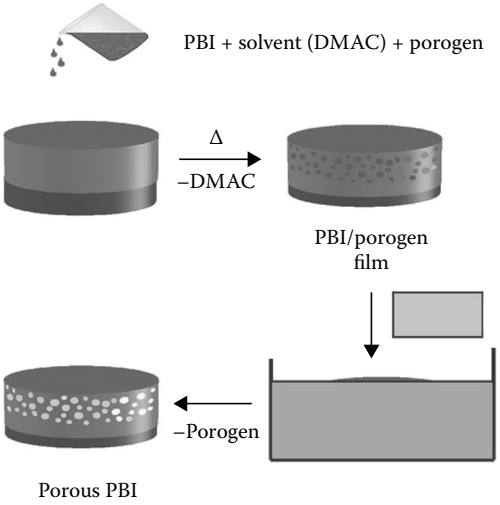

FIGURE 19.21 Synthesis of porous polybenzimidazole. (Reprinted with permission from D. Mecerreyes et al., *Chem. Mater.* 16: 604. Copyright 2004 American Chemical Society.)

Downloaded by [Yan Wang] at 17:51 05 January 2016

© 2016 by Taylor & Francis Group, LLC

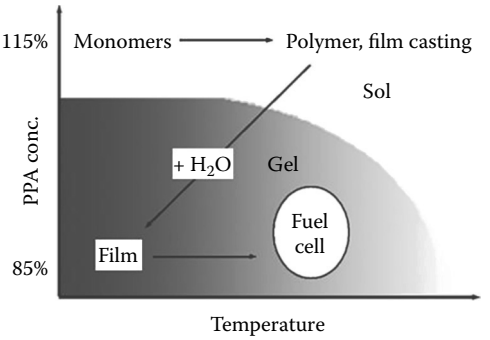

FIGURE 19.22 Sol–gel process state diagram. (Reprinted with permission from L. Xiao et al., *Chem. Mater.* 17: 5328. Copyright 2005 American Chemical Society.)

Downloaded by [Yan Wang] at 17:51 05 January 2016

atmosphere can readily hydrolyze the PPA to PA. The sol–gel transition is attributed to PBI's excellent solubility in PPA but poor solubility in PA. Membranes prepared using the PPA process demonstrate superior mechanical properties at higher levels of acid doping than membranes prepared using the previously mentioned acid-imbibing methods [93]. Not only do membranes produced through the PPA process have better mechanical properties at higher levels of acid doping, but also this process is much less tedious and time-consuming than the conventional imbibing method and porous PBI. Figure 19.22 illustrates the sol–gel transition observed via the PPA process.

19.7.2 Impact of Chemistry on Fuel Cell Performance

Like the morphology of a polymer gel film, the chemistry of the PBI membrane greatly impacts the properties of the gel film. Conductivity, acid doping levels, and the mechanical strength of the membrane are all affected by the chemistry of the polymer. Many PBI derivatives have been studied to assess and enhance these properties. The reader is directed to more complete reviews [14,87,89,94] on how various functional groups and differences in the polymer backbone affect the properties of PBI.

19.7.2.1 Meta-PBI

The first and most thoroughly studied PBI/PA complex is poly(2,2′-*m*-phenylene-5,5′-bibenzimidazole) or *m*-PBI, which can be seen in Figure 19.23a. This research was begun in 1995 by

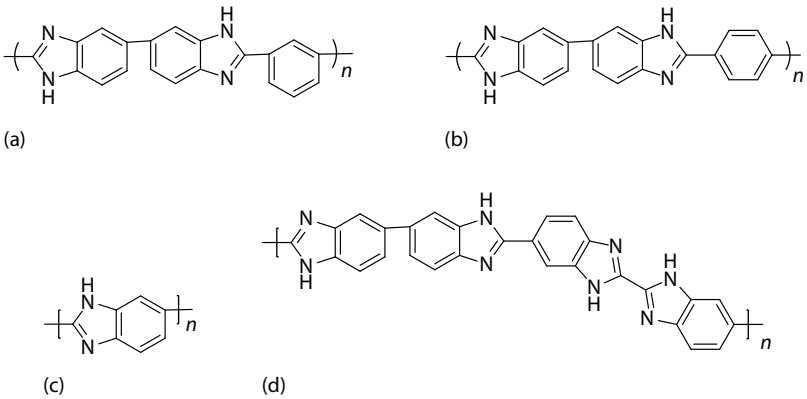

FIGURE 19.23 Chemical structures of various polybenzimidazoles: (a) *m*-PBI, (b) *p*-PBI, (c) AB-PBI, and (d) *i*-AB-PBI.

© 2016 by Taylor & Francis Group, LLC

Wainright et al., which focused on various synthetic and characterization methods of PBI [96]. During this research, it was discovered that a PBI membrane could be cast from a DMAc solution, imbibed with PA, and retain conductivity at high temperatures. This research ultimately led to nding that PBI had the potential for use as a membrane in fuel cells. Since then, many researchers have worked on characterizing *m*-PBI as well as other PBI derivatives.

19.7.2.1.1 Acid Doping Levels

Meta-PBI has been imbibed with PA using both the conventional method and the PPA process. The method through which the membrane is processed gives rise to different properties. One of the largest differences observed when comparing these processing methods is the acid doping level [ratio of moles of PA to moles of polymer repeat units (PA/PRU)], which greatly affects conductivity. When *m*-PBI is prepared through conventional imbibing, the acid doping level is typically 6–10 moles PA/PRU with conductivities ranging from 0.04 to 0.08 S cm^{-1} at 150°C at varying humidities [14,89]. Table 19.16 shows the conductivity at various levels of doping for *m*-PBI prepared through conventional imbibing including speci c testing conditions that have been reported [96–98]. When *m*-PBI is prepared through the PPA process, higher levels of acid doping are observed. Typical acid doping levels for *m*-PBI prepared through the PPA process range from 14 to 26 moles PA/PRU [14]. Conductivities of membranes prepared by the PPA process are typically higher than those prepared through conventional imbibing. In one report, it was observed that *m*-PBI prepared through the PPA process had a conductivity of 0.13 S cm^{-1} at 160°C under nonhumidi ed conditions [89]. Table 19.17 shows the conductivities at various temperatures for *m*-PBI prepared through the PPA process. To further compare the differences in the morphology of *m*-PBI prepared through conventional imbibing and the PPA process, membranes prepared through each method that had similar physical characteristics were compared. Although the acid doping levels are extremely close, the differences in conductivity and the proton diffusion coef cient can be seen in Table 19.18 [99]. These results demonstrate the differences in the proton transport architecture [89]. Not only does the membrane prepared through the PPA process have greater conductivity and proton architecture, but also the IV data show that higher-molecular-weight polymers are produced from the PPA process over the conventional method [89,93].

19.7.2.1.2 Fuel Cell Performance

Meta-PBI membranes doped through conventional imbibing have been tested many times for use in fuel cells. Li et al. [12] found that a membrane containing 6.2 moles PA/PRU reached a current

TABLE 19.16
IV, Acid Doping Levels, and Conductivity of Various *m*-PBI Membranes Prepared through Conventional Acid Imbibing

IV (dL g^{-1})	Acid Doping (PA/PRU)	Conductivity (S cm^{-1})	Operational Temperature (°C)	Relative Humidity	Reference
0.6	5.01	2×10^{-2}	130	NS	[96]
0.6	5	2.5×10^{-2}	150	NS	[96]
0.6	3.38	5×10^{-3}	130	NS	[96]
0.6	3.05	7×10^{-6}	30	NS	[97]
1.2	6.3	5×10^{-2}	140	30	[98]
1.2	6.3	2×10^{-2}	140	5	[98]
1.2	6.3	5.9×10^{-2}	150	30	[98]
1.2	6.3	4.7×10^{-3}	150	5	[98]

Source: W. J. Wainright et al., *J. Electrochem. Soc. 142*: L121, 1995; R. Bouchet and E. Siebert, *Solid State Ionics* 118: 287, 1999; J. A. Asensio et al., *J. Polym. Sci. Part A* 40: 3703, 2002.

Note: NS = not speci ed.

Downloaded by [Yan Wang] at 17:51 05 January 2016

© 2016 by Taylor & Francis Group, LLC

TABLE 19.17
Conductivity at Various Temperatures for *m*-PBI Prepared through the PPA Process

IV (dL g^{-1})	Acid Doping (PA/PRU)	Conductivity (S cm^{-1})	Temperature (°C)	Relative Humidity
1.49	14.4	5.16×10^{-2}	25	Dry
1.49	14.4	5.28×10^{-2}	40	Dry
1.49	14.4	6.23×10^{-2}	60	Dry
1.49	14.4	7.99×10^{-2}	80	Dry
1.49	14.4	9.52×10^{-2}	100	Dry
1.49	14.4	1.1×10^{-1}	120	Dry
1.49	14.4	1.2×10^{-1}	140	Dry
1.49	14.4	1.27×10^{-1}	160	Dry

Source: J. Mader et al., Polybenzimidazole/acid complexes as high-temperature membranes, *Fuel Cells II, Advances in Polymer Science* (G. G. Scherer, ed.), 216: 63, 2008.

TABLE 19.18
Comparison of *m*-PBI Prepared through Conventional Imbibing and PPA Process

Processing Method	Polymer (wt%)	Phosphoric Acid (wt%)	Water (wt%)	PA/PBI (Molar Ratio)	Conductivity (S cm^{-1})	Proton Diffusion Coefficient (cm^2 s^{-1})	IV (dL g^{-1})
Conventionally imbibed	15.6	60.7	23.7	12.2	0.048	10^{-7}	0.89
PPA process	14.4	63.3	22.3	13.8	0.13	3×10^{-6}	1.49

Source: D. C. Seel et al., High-temperature Polybenzimidazole-based Membranes, *Handbook of Fuel Cells*, pp. 300–312, 2009.

density of approximately 0.7 A cm^{-2} at 0.6 V at 190°C when hydrogen and oxygen gases were used under nonhumidi ed conditions. Figure 19.24 shows the fuel cell performance for *m*-PBI produced using the PPA process. Though performance was measured under high ow rate conditions, it shows its dependability at high temperatures [14]. Meta PBI has been used not only in PEM fuel cells but in direct methanol fuel cells (DMFCs) as well. When fed with 33.3 wt% methanol concentration and pure oxygen without back pressure, an open circuit voltage of 0.7 V and a maximum power density of 138.5 mW cm^{-2} at 200°C are reached, and durability tests show stable performance for over 120 h [91].

19.7.2.2 Para-PBI

Poly(2,2′-(*p*-phenylene)5,5′-bibenzimidazole) or *p*-PBI (Figure 19.23b) is one of the best performing PBI membranes for use in fuel cells [89]. Due to the rigid nature of its backbone, *p*-PBI was found to be dif cult to process. In 1975, high-molecular-weight (4.2 dL g^{-1}) *p*-PBI was synthesized by the US Air Force Materials Lab; however, the method required several weeks to produce high-molecular-weight polymer, and because it could not be spun into bers as easily as *m*-PBI, *p*-PBI was left unstudied for some time [89,100].

19.7.2.2.1 Acid Doping Levels

Kim et al. [101] produced *p*-PBI through both the PPA process and solution casting from methane sulfonic acid. When prepared through the PPA process, membranes were almost completely

Downloaded by [Yan Wang] at 17:51 05 January 2016

© 2016 by Taylor & Francis Group, LLC

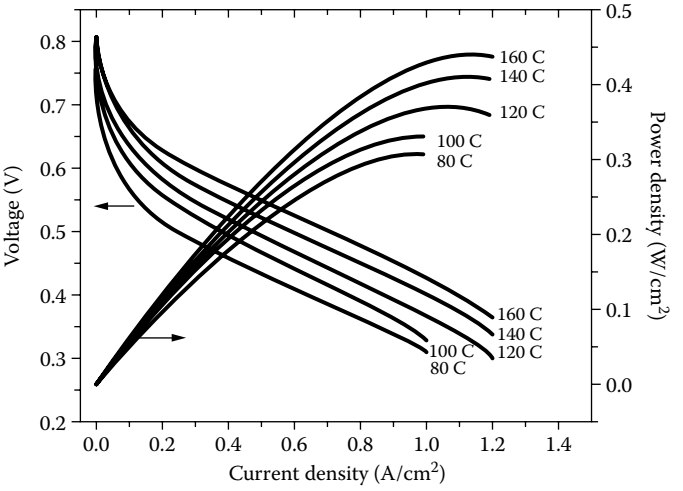

FIGURE 19.24 Performance curves of H_2/air *m*-PBI/PA fuel cells at various temperatures (1 atm absolute pressure). Operating conditions are as follows: constant ow rate, H_2 at 400 SCCM, air at 1300 SCCM, no humidi cation, 44 cm^2 active area, 1.0 mg cm^{-2} Pt catalyst loading, Pt–C 30% on each electrode. (From J. Mader et al., Polybenzimidazole/acid complexes as high-temperature membranes, *Fuel Cells II, Advances in Polymer Science* (G. G. Scherer, ed.), 216: 63, 2008.)

amorphous and showed much higher levels of acid doping and water uptake than when produced through solution casting [87]. Yu et al. [102,103] polymerized *p*-PBI through the PPA process at varying monomer concentrations. They had found the acid doping levels of *p*-PBI to be 30–40 PA/PRU [102,103]. When *p*-PBI produced through the PPA process had an acid doping level of 31.8 PA/PRU, a conductivity of 0.24 S cm^{-1} at 160°C was achieved. This shows that *p*-PBI has both a higher level of acid doping and a higher proton conductivity than *m*-PBI, which typically has 13–16 PA/PRU and a conductivity of 0.1–0.13 S cm^{-1} at 160°C [103]. It was also found that the monomer concentration (wt%) of *p*-PBI greatly affected the IV. This relationship can be seen in Figure 19.25. The IV of the PBI is important because it greatly affects the mechanical properties of the membrane (Figure 19.26). Since *p*-PBI demonstrates a high conductivity, high acid loadings, and good mechanical properties at high acid loadings, it is an excellent candidate for use in a PEM fuel cell.

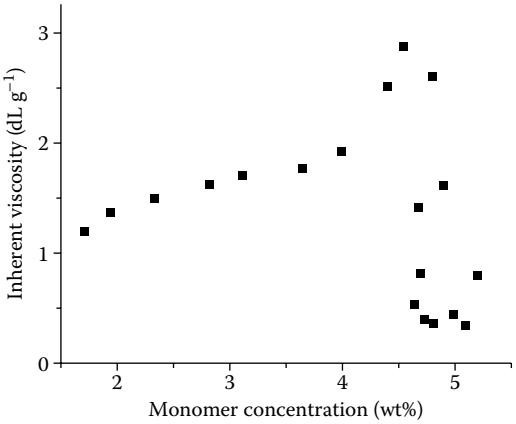

FIGURE 19.25 Effect of monomer concentration on the IV of *p*-PBI when polymerized at 195°C. (From S. Yu, *Fuel Cells* 9: 318, 2009.)

Downloaded by [Yan Wang] at 17:51 05 January 2016

© 2016 by Taylor & Francis Group, LLC

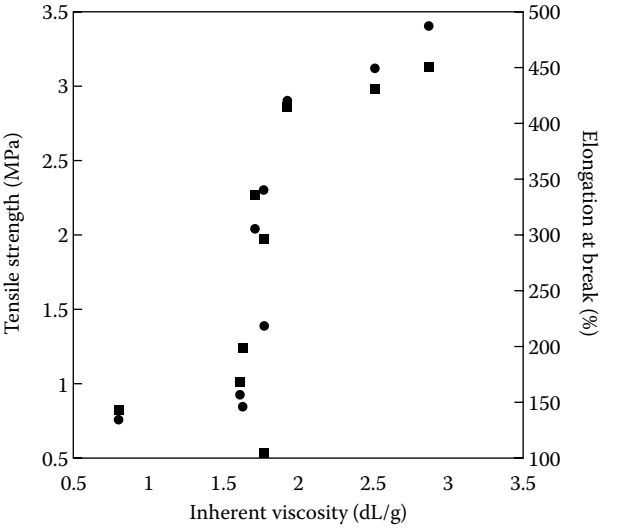

FIGURE 19.26 Effect of IV on tensile strength and elongation at break of *p*-PBI. IV measured using a Ubbelohde viscometer at a polymer concentration of 0.2 g/dL in concentrated sulfuric acid (96%) at 30°C. (Reprinted with permission from L. Xiao et al., *Chem. Mater.* 17: 5328. Copyright 2005 American Chemical Society.)

19.7.2.2.2 Fuel Cell Performance

The polarization curves for *p*-PBI membrane is shown in Figure 19.27. This fuel cell was operated under nonhumidi ed conditions using hydrogen and air as the fuel and oxidant. The voltage increased from 0.606 to 0.663 V when the temperature was increased from 120°C to 180°C at 0.2 A cm^{-2} [103]. This demonstrates that *p*-PBI can operate at high temperatures without the need for humidi cation due to the involvement of PA in the proton conduction mechanism. Fuel cell durability tests were also performed for *p*-PBI. To test long-term durability, temperature and current

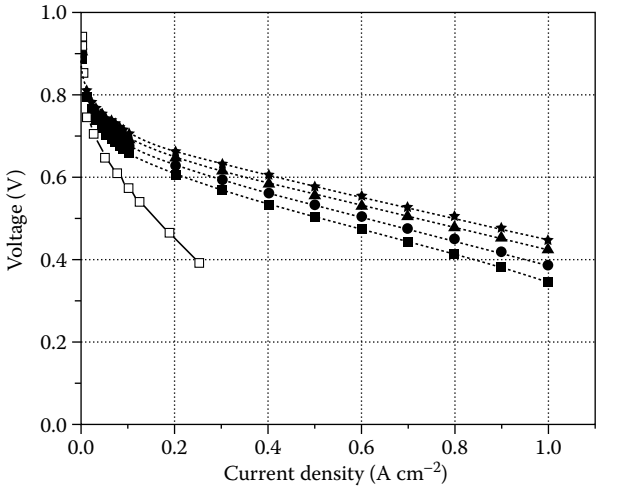

FIGURE 19.27 Polarization curves for membrane-based fuel cells with *p*-PBI membranes using 1.2–2.0 stoichiometric ows, respectively, at ambient pressure (1 atm, absolute). Squares: 120°C, circles: 140°C, triangles: 160°C, and stars: 180°C. (Open squares: m-PBI data at 150°C adapted from Wang et al., *Electrochim. Acta* 1996, 41, 193. From S. Yu, *Fuel Cells* 9: 318, 2009.)

Downloaded by [Yan Wang] at 17:51 05 January 2016

© 2016 by Taylor & Francis Group, LLC

density (0.2 A cm^{-2}) were held constant, and the voltage was recorded. Hydrogen and air were used as the fuel and oxidant at stoichiometric flows of 1.2 and 2.0, respectively [102]. The voltage was monitored at 80°C, 160°C, and 190°C to ensure durability testing over a wide range of temperatures. For the study at 80°C, the fuel cell was first broken in for 80 h and operated at 120°C. It was then run for over 900 h at 80°C and a voltage degradation rate of 45 μV h^{-1}. The performance test that had taken place at 160°C showed a voltage degradation of 4.9 μV over a 2500 h period. When tested at 190°C, the voltage degradation was found to be 60 μV h^{-1}, which shows to be significantly higher than the voltage degradation at 160°C. This could be due to multiple factors such as Pt dissolution, Pt agglomeration, and carbon support corrosion [102].

19.7.2.3 AB-PBI

The simplest known structure of PBI that can be prepared using commercial monomers is poly(2,5-benzimidazole) or AB-PBI (Figure 19.23c) [104]. This polymer is prepared using only the monomer 3,4-diaminobenzoic acid because it contains both the diamine and acid functionalities. In addition to the homopolymer, copolymers, cross-linked polymers, and substituted polymers containing AB-PBI have been studied [105]. AB-PBI has been prepared through both conventional imbibing and the PPA process.

19.7.2.3.1 Acid Doping Levels

When prepared through conventional imbibing, acid doping levels are between 2 and 10 mol PA/PRU and demonstrate a conductivity of approximately 0.05 S cm^{-1} at 180°C under anhydrous conditions [106]. It is important to note that unlike the previously mentioned *m*-PBI and *p*-PBI, AB-PBI contains one benzimidazole per repeat unit rather than two. This must be taken into consideration when comparing acid doping levels of different PBI chemistries. AB-PBI prepared using the PPA process demonstrates higher levels of acid doping (22–35 mol PA/PRU) than when prepared through conventional imbibing [14]. The optimal monomer concentration was found to be approximately 3 wt% and yielded an IV of 4.63 dL g^{-1}. These membranes, however, were found to be thermally unstable at temperatures greater than 130°C. Adjusting the PA level was done by soaking the membranes in PA baths with lower concentrations of PA in the original film [105]. These films containing lower levels of PA (14.5, 22.7, and 29.1 mol PA/PRU) were still unstable at high temperatures; therefore, conductivity and fuel cell performance were unable to be measured when prepared through the PPA process [105].

19.7.3.3.2 Isomeric AB-PBI

In 2011, a new sequence isomer of AB-PBI was reported (Figure 19.23d) [105]. This new sequence, *i*-AB-PBI, contains head-to-head, head-to-tail, and tail-to-tail linkages of the 2,5-benzimidazole groups unlike AB-PBI, which contains only head-to-tail linkages or benzimidazole-to-phenyl linkages. By inducing a new sequence in the AB polymer, two new types of bonds were added: benzimidazole-to-benzimidazole and phenyl-to-phenyl bonds. To induce this sequence change, a novel monomer, 2,2′-bisbenzimidazole-5,5′-dicarboxylic acid (Figure 19.28), was prepared and polymerized with 3,3′4,4′-tetraaminobiphenyl through the PPA process. Acid doping levels were reportedly 24–37 moles PA/PRU. The optimal monomer concentration for *i*-AB-PBI was found to be approximately 6 wt%. At this weight percentage, IVs were ~3 dL g^{-1} and showed conductivities of

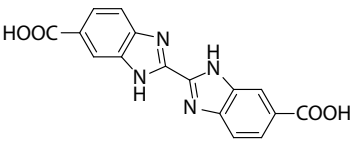

FIGURE 19.28 Chemical structure of 2,2′-bisbenzimidazole-5,5′-dicarboxylic acid.

Downloaded by [Yan Wang] at 17:51 05 January 2016

© 2016 by Taylor & Francis Group, LLC

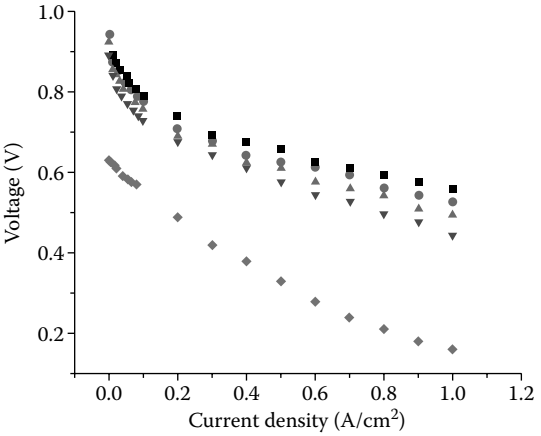

FIGURE 19.29 Polarization curves for *i*-AB-PBI membranes with stoichiometric ows of 1.2:2.0 hydrogen/oxygen, respectively. (Squares: 180°C, circles: 160°C, triangles: 140°C, inverted triangles: 120°C, diamonds: reference data S. Yu et al., *Fuel Cells* 8: 165, 2008 for AB-PBI at 130°C.) (From A. L. Gulledge et al., *J. Polym. Sci. Part A* 50: 306, 2012.)

Downloaded by [Yan Wang] at 17:51 05 January 2016

>0.2 S cm^{-1} [105]. The conductivities are signi cantly higher than the conductivities of AB-PBI. Due to the high conductivity of *i*-AB-PBI, it was a good candidate for fuel cell testing. Figure 19.29 shows the polarization curve for *i*-AB-PBI and gives a comparison to AB-PBI. When fuel cell performance was evaluated using *i*-AB-PBI, the output voltage was found to be 0.65 V at 0.2 A cm^{-2} at 180°C when operating under hydrogen and air [105]. This was conducted over a period of 3500 h. These results show that *i*-AB-PBI is a promising candidate for use in high-temperature PEM fuel cells.

19.8 PBI-BASED MEMBRANES FOR PERVAPORATION SEPARATION

Because of their outstanding chemical resistance and mechanical and thermal stability, PBI membranes were used not only in high-temperature PEM fuel cells but also for many other separation applications such as RO [44–46,106–110], nano ltration (NF) [111–114], ultra ltration [115], forward osmosis [81,114], pervaporation [27,116–123], and gas separation [62,83,124–138], particularly for applications in aggressive environments.

Since the early 1970s, PBI membranes have been developed for RO and hemodialysis applications. Model et al. [44–46], as well as Brinegar [106], summarized most of the early development. Table 19.19 illustrates a comparison between PBI and cellulose acetate (CA) membranes for RO

TABLE 19.19
Comparative Performance of PBI and CA RO Membranes

Operating Temp. (°C)	Testing Time (h)	Final Flux of CA Membranes (gal/ft²-day)	Final Flux of PBI Membranes (gal/ft²-day)
70	5	12	16
120	5	20	17
167	20	5	19
194	5	0	25

Source: F. S. Model and L. A. Lee, PBI reverse osmosis membranes: An initial survey, *Reverse Osmosis Membrane Research* (H. K. Londale and H. E. Podall, eds.), Plenum Press, New York, p. 285, 1972.

© 2016 by Taylor & Francis Group, LLC

application [45]. It shows that PBI has comparable RO performance as compared to CA at ambient temperatures, but outperforms CA at elevated temperatures; this is the uniqueness of PBI membranes. In the 1980s, Sawyer and Jones [107] reported the detailed morphologies of low- ux and high- ux PBI membranes, whereas Bower and Rafalko [108] as well as Sansone [109] at Hoechst Celanese invented N-substituted or ethylene-carbonated modi ed PBIs for RO and ultra ltration applications. Calundann and Chung [110] developed microporous PBI membranes with a narrow pore size distribution. PBI NF membranes have also been developed recently [111–113] for the removal of heavy metal ions and pharmaceutical residuals from wastewater. Here we will only focus on PBI applications as the membrane material for pervaporation applications in this section and gas separations in Section 19.9.

Pervaporation is a membrane-based technique for liquid separation. The liquid feed solution is circulated and in direct contact with the upstream side of the membrane, while vacuum or inert gas is applied on the downstream side of the membrane. The driving force for the feed component to transport through the membrane is the chemical potential (partial vapor pressure) difference of the components between the feed and permeate sides. Thus, the separation is achieved by the differences in the diffusivities and solubilities of the components. Compared with those conventional techniques such as distillation, liquid–liquid extraction, etc., pervaporation has much higher separation ef ciency, low energy consumption, simple equipment, low capital cost, and no pollution. The key factor of the pervaporation separation technology lies in the membrane. Its structure and physicochemical properties play determining factors on the pervaporation performance. In addition to achieving good selectivity and permeability, a desirable pervaporation membrane material must have good chemical and thermal stability in order to survive in the harsh environment.

As a high-performance aromatic polymeric material, many PBI membranes have been reported for pervaporation separation recently [27,116–123] for organic dehydration such as EG, acetone, acetic acid, etc., as well as some organic–organic separation. The rigid chemical structure, high hydrophilicity, and good spinnability all make PBI a promising membrane material for pervaporation dehydration. Besides, PBI is known to absorb 15 wt% water at equilibrium, and the water in PBI is mobile [48]. Therefore, water can preferentially permeate the PBI membrane due to its stronger af nity with PBI molecules and smaller molecular size relative to most organics in pervaporation dehydrations.

19.8.1 PBI-Based Membranes with Various Modifications

In spite of the many advantages of PBI, it has some weaknesses: (1) thin phase-inversed PBI membranes are brittle after drying; (2) PBI membranes can be easily swollen in aqueous solutions, resulting in a decreased membrane selectivity and unstable long-term performance; and (3) the high cost of PBI is another issue. Various modi cation methods including cross-linking, surface modi cation, blending, and thermal treatment have been proposed to overcome these issues and produce useful PBI membranes for pervaporation as follows.

19.8.1.1 Cross-Linking

P-xylene dichloride was employed as a cross-linking agent for the PBI selective layer of the PBI/P84 dual-layer hollow bers in a recent study for acetone dehydration [119]. The cross-linking mechanism involves a reaction between the N–H functional groups of PBI molecules and the chlorine functional group of *p*-xylene dichloride to form the 1-methylimidazole groups as illustrated in Figure 19.30 [112]. Using a feed solution of 85/15 wt% acetone/water at 50°C, the pervaporation results demonstrated that the cross-linking modi cation can improve the separation factor signi cantly to 498 from 7.19 of the uncross-linked membrane, while the ux decreased to 300 g/m^{2}·h from 1243 g/m^{2}·h. Clearly, the cross-linking modi cation can reduce the PBI membrane swelling and result in an enhanced pervaporation membrane for acetone–water separation.

Downloaded by [Yan Wang] at 17:51 05 January 2016

© 2016 by Taylor & Francis Group, LLC

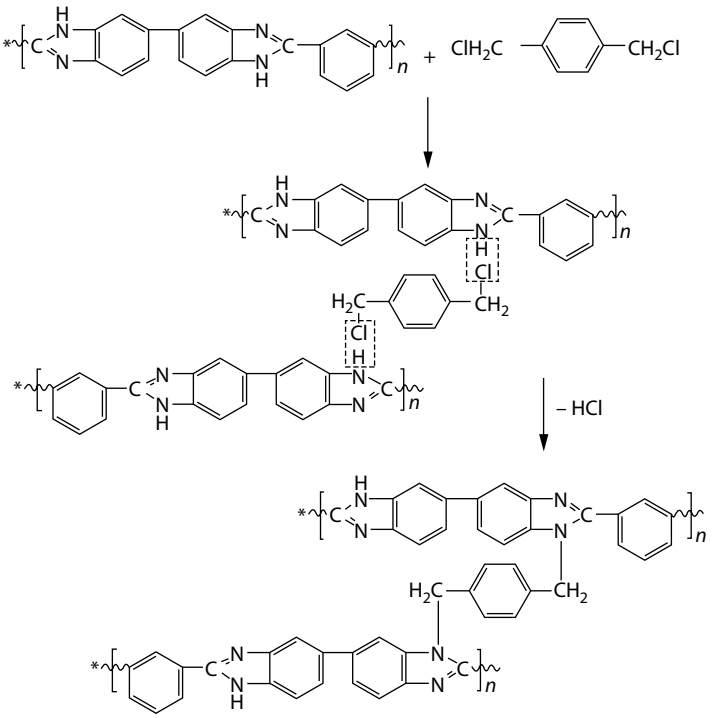

FIGURE 19.30 Proposed mechanism for the chemical cross-linking modi cation of PBI using *p*-xylene dichloride. (Reprinted from *Chem. Eng. Sci*., 61, K. Y. Wang, Y. C. Xiao, and T. S. Chung, Chemically modi ed polybenzimidazole nano ltration membrane for the separation of electrolytes and cephalexin, 5507, Copyright 2006, with permission from Elsevier.)

19.8.1.2 Sulfonation

Sulfonation modi cation of the PBI membrane surface was conducted recently by Wang et al. [116] for acetic acid dehydration. Figure 19.31 illustrates the sulfonation mechanism. Successful attachment of sulfonate groups to the imidazole ring of the PBI membrane not only enhances membrane hydrophilicity but also lowers the membrane's af nity toward acetic acid. As a result, both the ux and separation factor are enhanced signi cantly. The best pervaporation performance of the sulfonated PBI membrane

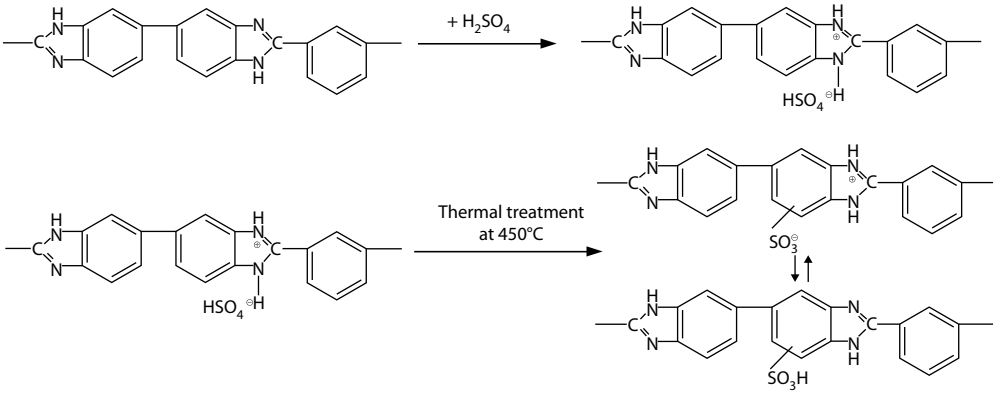

FIGURE 19.31 Sulfonation mechanism of PBI material. (Reprinted from *J. Membr. Sci*., 415–416, Y. Wang, T. S. Chung, and M. Gruender, Sulfonated polybenzimidazole membranes for pervaporation dehydration of acetic acid, 486, Copyright 2012, with permission from Elsevier.)

Downloaded by [Yan Wang] at 17:51 05 January 2016

© 2016 by Taylor & Francis Group, LLC

has a ux of 207 g/m^2·h and a separation factor of 5461 for the dehydration of a 50/50 wt% acetic acid/water feed solution at 60°C, which not only outperforms the conventional distillation process but also surpasses most other polymeric pervaporation membranes reported in the literature.

19.8.1.3 Polymer Blending

PBI/Matrimid (a commercial PI) blend membranes have been reported for the pervaporation dehydration of *tert*-butanol [122] and the separation of toluene/iso-octane mixture [27]. Because of hydrogen bonding interaction between the functional groups of these two polymers (Figure 19.32), PBI and Matrimid are completely miscible in all compositions at the molecular level. The incorporation of a small amount (up to 3.55%) of PBI into Matrimid was found to improve membrane hydrophilicity and stabilize Matrimid's chains for high-temperature pervaporation. As a consequence, the blend membrane has higher separation performance for the dehydration of *tert*-butanol/water mixtures. Similar improving mechanisms can be observed for the toluene/iso-octane separation by Kung et al. [27] using blend hollow ber membranes. The hollow ber comprising 10 wt% of PBI exhibits the best performance with a separation factor of 200 and a ux of 1.35 kg/m^2·h for a feed solution of 50/50 wt% toluene/iso-octane at 60°C. The PBI/Matrimid blend may also have better compatibility with toluene, which favors the solubility selectivity of toluene over iso-octane.

19.8.1.4 Mixed-Matrix Membranes

Mixed-matrix membranes (MMMs) formed by incorporating as-synthesized wet-state ZIF nanoparticles into the PBI matrix have been studied by Shi et al. [120,121] for alcohol dehydration. ZIF-8 nanoparticles, with their high thermal stability, chemical resistance, and excellent compatibility with PBI, have shown their great potential to enhance PBI separation performance. Unlike most conventional MMMs, a homogeneous distribution of ZIF nanoparticles in the PBI matrix could be observed with the ZIF content not exceeding 58 wt% (as shown in Figure 19.33). This is due to the fact that the same solvent (i.e., NMP) is used, and both ZIF-8 and PBI molecules contain common imidazole functional groups. Compared with neat PBI membranes, PBI/ZIF-8 MMMs with 33.7 wt% ZIF-8 showed a fourfold increase in the water permeability (from 11.6 to 81 g/m^2 h) and a relative stable selectivity of about 3400 for the dehydration of 85 wt% *n*-butanol aqueous solution at 60°C [120]. The great improvement with the aid of ZIF nanoparticles in separation performance was contributed by (1) the reduction in the transport energy barrier of penetrants and (2) the suppressed solvent-induced swelling. By means of positron annihilation lifetime spectroscopy (PALS), it was found that the free volume diameter of the PBI membrane increased slightly from 4.56 to 4.78 Å together with a substantial increase in the fractional free volume (FFV) from 1.64% to 5.22% because of large cavities of ZIF-8 particles. Therefore, the MMMs have higher pervaporation permeability. In addition, sorption data con rmed that the ethanol-, methanol- and water-induced

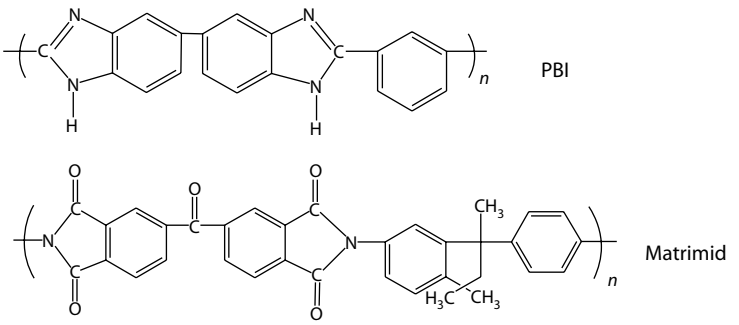

FIGURE 19.32 Hydrogen bonding interaction between PBI and Matrimid. (Reprinted from *J. Membr. Sci.*, 271, T. S. Chung, W. F. Guo, and Y. Liu, Enhanced matrimid membranes for pervaporation by homogeneous blends with polybenzimidazole (PBI), 221, Copyright 2006, with permission from Elsevier.)

Downloaded by [Yan Wang] at 17:51 05 January 2016

© 2016 by Taylor & Francis Group, LLC

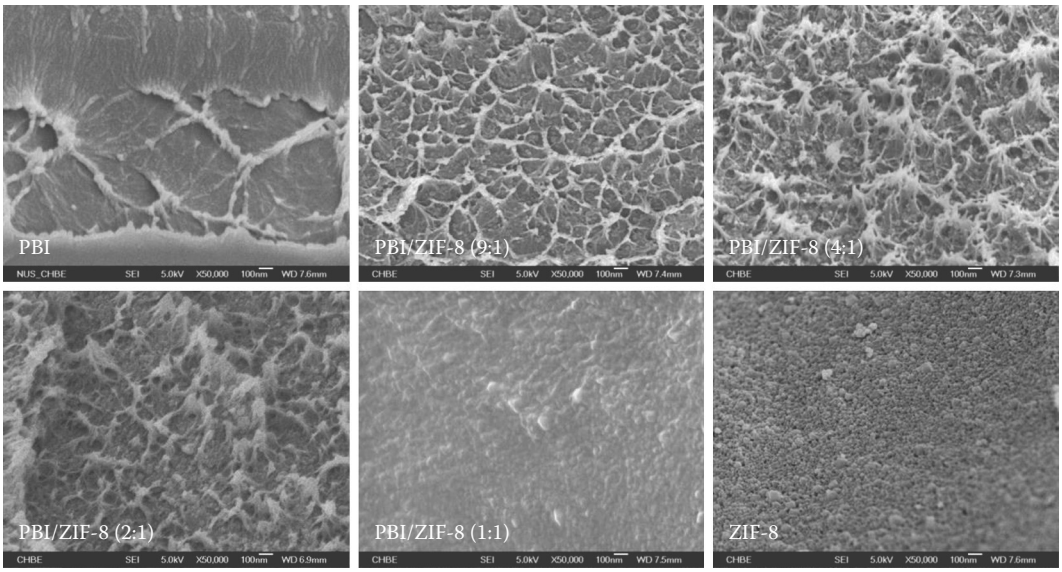

FIGURE 19.33 FESEM morphologies of PBI/ZIF-8 membranes with various ZIF-8 loadings. (Reprinted from *J. Membr. Sci.*, 415–416, G. M. Shi, T. Yang, and T. S. Chung, Polybenzimidazole (PBI)/zeoliticimidazolate frameworks (ZIF-8) mixed-matrix membranes for pervaporation dehydration of alcohols, 577, Copyright 2010, with permission from Elsevier.)

membrane swelling, especially the water-induced swelling, could be effectively suppressed in the MMMs because of the hydrophobic nature and rigid structure of ZIF-8 particles [121].

19.8.2 PBI Hollow Fiber Membranes

Compared with flat-sheet membranes, hollow fiber membranes exhibit substantial enhancement in the permeation flux because of the provision of larger surface area, less transport resistance, and lower swelling. Additionally, hollow fibers have self-contained vacuum channels where the feed can be supplied from the shell side while vacuum is applied from the lumen side, or vice versa. The porous and vacuum-dry substructure of asymmetric hollow fibers also helps reduce the swelling in the selective layer, and thus achieves a higher separation factor.

Recently, three types of PBI membranes were developed for pervaporation dehydration of EG [117,118], namely, dense flat-sheet PBI membranes and PBI single-layer and PBI/polyetherimide (PEI) dual-layer hollow fiber membranes. PBI flat-sheet dense membranes had the lowest separation performance due to the dense morphology and severe swelling. The single-layer PBI hollow fibers showed much improved separation performance in both permeation flux (1147 $g/m^2 \cdot h$) and separation factor [116], but they had very low tensile strains and were very fragile. It was difficult to fabricate modules from these weak fibers. The PBI/PEI dual-layer hollow fiber membranes had the best separation performance due to the unique combination of both material strengths and physicochemical properties of the PBI outer selective layer and the less swelling characteristics of the PEI supporting layer via dual-layer coextrusion. The developed PBI/PEI dual-layer hollow fiber membrane had a separation factor up to 4500 and a flux up to 186 g/m^2 h, which were far better than most other polymeric membranes [117]. Figure 19.34 shows its morphology.

PBI/P84 dual-layer hollow fiber membranes were also developed for pervaporation dehydration of tetrafluoropropanol (TFP) [123] and acetone [119] using P84 co-polyimide as the support layer. Besides good solvent resistance and thermal stability, P84 has excellent antiswelling properties and good compatibility with PBI. The PBI/P84 membrane has superior separation performance to both the PBI single-layer and P84 single-layer hollow fiber membranes. Clearly, there is great perspective

Downloaded by [Yan Wang] at 17:51 05 January 2016

© 2016 by Taylor & Francis Group, LLC

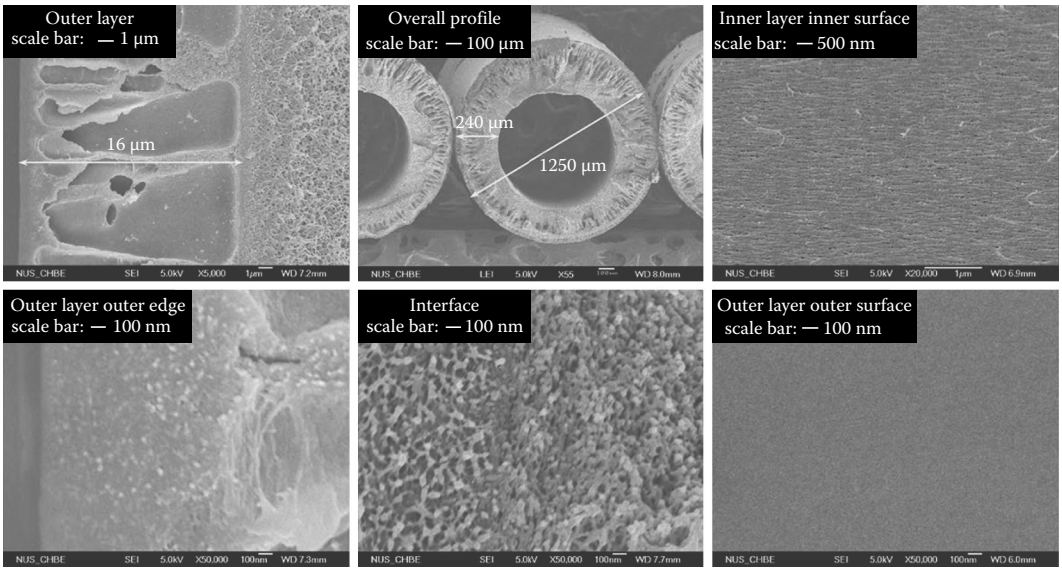

FIGURE 19.34 FESEM images of the membrane morphology of PBI/PEI dual-layer hollow fibers. (Reprinted from *J. Membr. Sci.*, 363, Y. Wang, M. Gruender, and T. S. Chung, Pervaporation dehydration of ethylene glycol through polybenzimidazole (PBI)-based membranes. 1. Membrane fabrication, 149, Copyright 2010, with permission from Elsevier.)

to develop PBI dual-layer hollow fiber membranes for pervaporation separations by using other materials as substrates. Not only can it reduce the PBI material cost, but also it can enhance the overall separation performance.

19.9 PBI-BASED MEMBRANES FOR GAS SEPARATION

PBI-based membranes have emerged as gas separation membranes for energy-related applications such as precombustion and postcombustion CO_2 capture, nitrogen/oxygen separation, acid gas removal from natural gas, separation of hydrogen from its mixtures with nitrogen, CO_2, CO, or hydrocarbons, and others.

Gas transport across polymeric membranes follows the solution-diffusion mechanism, and the gas permeability is a product of diffusion coefficient and solubility coefficient. For industrial gas separation, separation at high temperatures is advantageous since neither cooling step nor energy loss would be involved. However, most commercial polymers cannot survive at high temperatures. This makes PBI a promising membrane material for gas separation at elevated temperatures exceeding 150°C. Not only does it have remarkable thermal stability, but also it has notably high intrinsic gas-pair selectivity. PBI has a low gas permeability at room temperature, but its rigid structure makes it suitable for diffusivity-based separations at high temperatures.

In order to develop a high-performance PBI membrane for gas separation, various molecular design and modifications were proposed to improve its low gas permeability, such as monomer optimization [124,125], N-substitution [126–128], chemical cross-linking [62,129], polymer blending [62,130,131], hollow fiber engineering [129,131,132], and addition of inorganic particles [133–138].

19.9.1 Monomer-Level Optimization

By hindering chain packing and inhibiting chain flexibility simultaneously, attempts have been made to molecularly optimize the monomers for PBI syntheses [124,125]. Figure 19.35 shows the chemical structures of some selected PBI polymers, and their corresponding gas separation performance

Downloaded by [Yan Wang] at 17:51 05 January 2016

© 2016 by Taylor & Francis Group, LLC

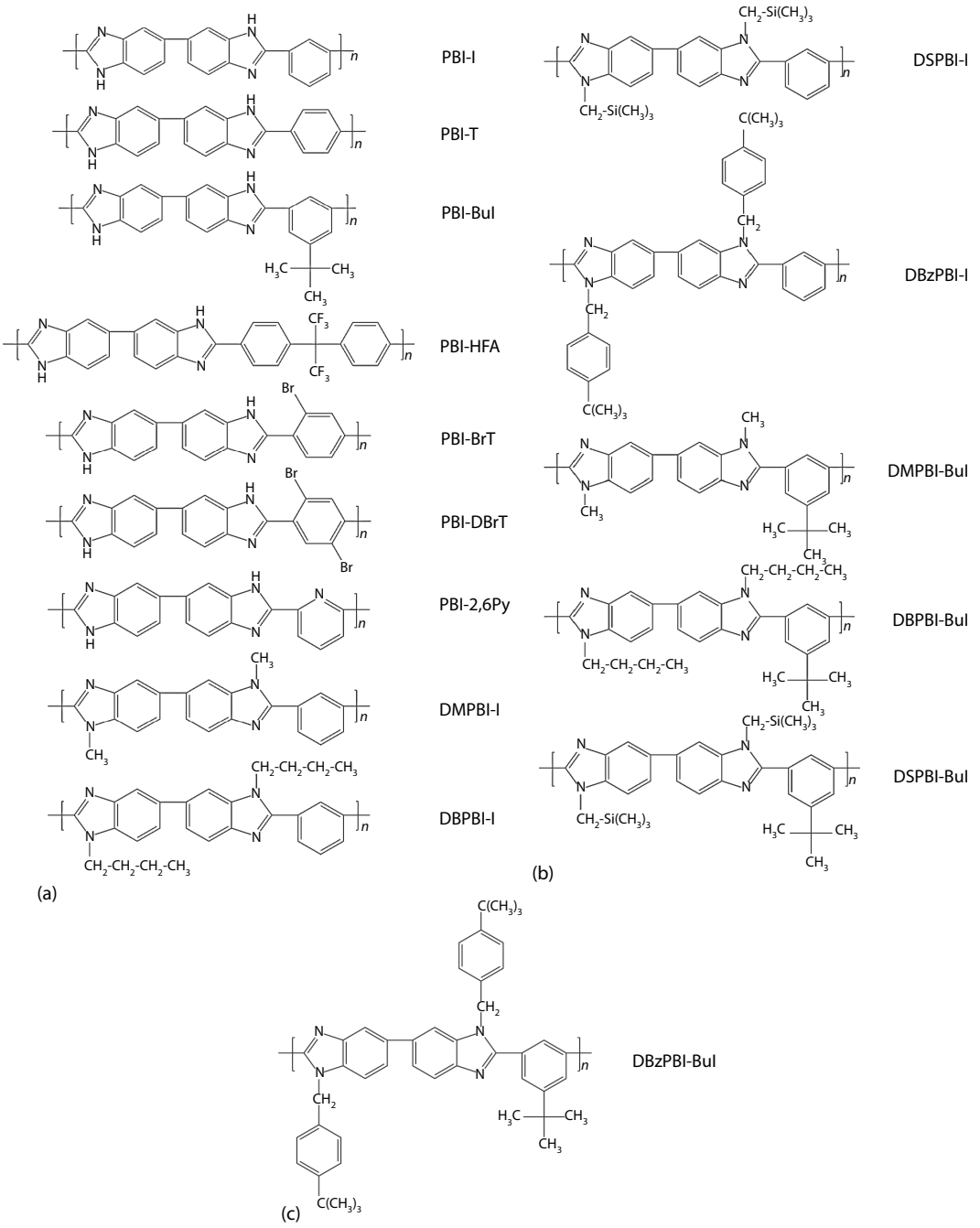

FIGURE 19.35 Chemical structures of PBIs in Table 19.20: (a) PBIs synthesized from 3,3'-diaminobenzidine (DAB) and dicarboxylic acid, (b) PBI-I with N-substitutions, and (c) PBI-BuI with N-substitutions.

is given in Table 19.20. By introducing bulky groups to some polymer chains, free volumes increase without serious loss in the chain rigidity; thus, modi ed PBI membranes have higher gas permeability.

Through the variation of the acid moiety during polymer syntheses, the optimized PBI polymers showed a reduced chain packing density and better solvent solubility, but slightly lower thermal stability [124,125]. For example, PBI made from 4,4′-(hexa uoroisopropylidene)bis(benzoic acid) (HFA)

Downloaded by [Yan Wang] at 17:51 05 January 2016

© 2016 by Taylor & Francis Group, LLC

© 2016 by Taylor & Francis Group, LLC

Downloaded by [Yan Wang] at 17:51 05 January 2016

TABLE 19.20
Gas Separation Performance of Pristine PBI Membranes

		Permeability (Barrer)					Selectivity				
Material	***P* (atm)**	**H_2**	**CO_2**	**O_2**	**N_2**	**CH_4**	**H_2/CO_2**	**CO_2/N_2**	**CO_2/CH_4**	**H_2/O_2**	**Reference**
PBI-I	19.4	0.63	0.16	0.015	0.0048	0.0018	3.8	33.0	89.0	42.0	[125,126]
PBI-T	19.4	0.16	–	0.004	–	–	–	–	–	55.0	[125]
PBI–BuI	19.4	10.66	1.91	0.42	0.06	0.05	5.58	32.0	37.0	25.4	[124,125]
PBI–HFA	19.4	12.15	2.91	0.60	0.13	0.07	4.18	22.0	41.0	20.1	[124,125]
PBI–BrT	19.4	0.38	–	0.006	–	–	–	–	–	60.0	[125]
PBI–DBrT	19.4	1.89	–	0.07	–	–	–	–	–	28.0	[125]
PBI–2,6Py	19.4	1.38	–	0.045	–	–	–	–	–	31.0	[125]
DMPBI-I	19	2.18	0.19	0.052	0.005	–	11.3	38.7	–	41.9	[126,128]
DBPBI-I	19	6.54	1.79	0.36	0.09	0.06	3.7	20.0	32.4	18.2	[126,128]
DSPBI-I	19	6.81	1.62	0.38	0.07	0.04	4.2	22.1	43.0	17.9	[126,128]
DBzPBI-I	19	22.85	6.24	1.73	0.43	0.23	3.7	14.5	26.8	13.2	[126,128]
DMPBI-BuI	19	13.06	5.62	0.91	0.21	0.15	2.3	27.2	37.8	14.4	[126,128]
DBPBI-BuI	19	26.90	9.11	2.39	0.56	0.46	3.0	16.3	19.7	11.3	[126,128]
DSPBI-BuI	19	39.16	7.81	3.50	0.71	0.63	5.0	11.0	12.3	11.2	[126,128]
DBzPBI-BuI	19	46.45	21.32	6.27	1.51	1.37	2.2	14.1	15.5	7.4	[126,128]

Note: Testing temperature: 35 °C; *P*, transmembrane pressure; 1 Barrer = 1×10^{-10} cm^3 (STP) cm cm^{-2} s^{-1} cm Hg^{-1}.

(PBI-HFA) exhibited a H_2 permeability of 12.2 Barrer at 35°C, which was an increment of nearly 20-fold as compared to the conventional PBI [124]. However, since the glass transition temperature (T_g) of PBI-HFA dropped to 330°C (i.e., a T_g drop of 86°C from the conventional PBI of 416°C), there are modest decreases in its thermal stability and gas selectivity for industrial applications at high temperatures.

19.9.2 N-Substitution Modification

Similar to the aforementioned monomer-level optimization, the postmodification by N-substitution [126–128] is an effective modification method to improve the gas permeability of PBI membranes. By incorporating bulky side groups, the N-substitution aimed to break the intermolecular hydrogen bonding and disrupt chain packing so that the physicochemical and gas permeation properties can be enhanced. For example, both the glass transition temperature and degradation temperature of N-substituted AB-PBI dropped due to the increase in chain flexibility [127]. In spite of the decline in gas selectivity, the increase in gas permeability was observed. Gas sorption capability also increased because of the looser chain packing with the inclusion of bulky alkyl groups and weaker hydrogen bonding interactions. Solubility enhancement in some common solvents (chloroform, trichloroethylene, etc.) were also noticed.

19.9.3 Chemical Cross-Linking

Similar to previous Section 19.8.1.1, cross-linking generally leads to a higher selectivity but a lower permeability. For H_2/CO_2 gas separation [62], the *p*-xylene dichloride and *p*-xylene diamine cross-linked PBI/Matrimid blend membranes showed H_2/CO_2 selectivity of 9.43 and 26.09, respectively. Since the chemical modification may occur mainly at the PBI phase (by *p*-xylene dichloride) or the Matrimid phase (by *p*-xylene diamine), it gives us the freedom to manipulate gas pair selectivity with different chain packing density and segmental mobility.

In another study, the cross-linked PBI-HFA membranes [124] showed substantial improvement in gas selectivity but simultaneously decreased gas permeability as compared to the uncross-linked membranes.

19.9.4 Polymer Blending

Table 19.21 tabulates the gas separation performance of some selected PBI blend membranes. In the case of PBI/Matrimid blend membranes [62,130,131], the incorporation of PBI into the Matrimid matrix resulted in a higher gas selectivity but a lower gas permeability. The enhancement in selectivity is mainly attributed to a higher diffusivity selectivity since PBI has a higher molecular sieving effect, while the decline in permeability is due to the reduction in FFV and *d*-spacing. The formation of strong hydrogen bonding between blend components may also contribute to the diminishment of FFV. Delamination-free PBI/Matrimid blend dual-layer hollow fiber membranes were developed for gas separation [131]. With the aid of chemical cross-linking modification, the dual-layer hollow fiber membranes have a H_2/CO_2 selectivity of about 14.49.

Carbon molecular sieve membranes were also made from various PBI/PI blends [130]. Carbon membranes derived from PBI/Matrimid precursors exhibited better gas separation performance than other two blend precursors, namely, PBI/Torlon and PBI/P84. The newly developed PBI-based carbon membranes surpassed the trade-off lines and were of great potentials for industrial applications. The selectivity of CO_2/CH_4 and H_2/CO_2 reaches 203.95 and 33.44, respectively, while for the N_2/CH_4 separation, an unprecedented high N_2 permeability of 2.78 Barrer is achieved with a high selectivity of 7.99.

19.9.5 Mixed-Matrix Membranes

MMMs have also been proposed to overcome the low permeability of PBI-based gas membranes. Some of them and their gas separation performance are listed in Table 19.21. The key to fabricate

Downloaded by [Yan Wang] at 17:51 05 January 2016

© 2016 by Taylor & Francis Group, LLC

© 2016 by Taylor & Francis Group, LLC

Downloaded by [Yan Wang] at 17:51 05 January 2016

TABLE 19.21
Gas Separation Performance of PBI Blends and MMMs

Material	T (°C)	P (atm)	Permeability (Barrer)				Selectivity			Reference
			H_2	CO_2	N_2	CH_4	H_2/CO_2	CO_2/N_2	CO_2/CH_4	
Matrimid/PBI (75/25 wt%)	35	10	19.72	4.19	0.163	0.13	4.1	25.7	32.2	[62]
Matrimid/PBI (50/50 wt%)	35	10	13.06	2.16	0.072	0.045	6.1	30	48	[62]
Matrimid/PBI (25/75 wt%)	35	10	5.47	0.58	0.021	0.0097	9.4	27.6	59.8	[62]
PBI/PAMH (14 wt%) (proton-exchanged AMH-3, silicate)-2	35	–	1	0.025	–	–	40	–	–	[133]
PBI/PAMH (14 wt%) (proton-exchanged AMH-3, silicate)-2	200	–	18	0.82	–	–	22	–	–	[133]
PBI/SAMH (3 wt%) (swollen AMH-3, silicate)	35	–	0.9	0.03	–	–	34	–	–	[133]
PBI/SAMH (3 wt%) (swollen AMH-3, silicate)	200	–	15	0.71	–	–	21	–	–	[133]
PBI/SAMH (2 wt%) (swollen AMH-3, silicate)	35	–	1.5	0.04	–	–	34	–	–	[133]
PBI/SAMH (2 wt%) (swollen AMH-3, silicate)	200	–	18	1	–	–	18	–	–	[133]
PBI/ZIF-7 (13.7 wt%)	35	3.5	7.7	0.60	–	–	12.9	–	–	[135]
PBI/ZIF-7 (26.1 wt%)	35	3.5	15.4	1.3	–	–	11.9	–	–	[135]
PBI/ZIF-7 (26.1 wt%) (mixed gas)	180	3.5	221	26.3			8.4			[135]
PBI/ZIF-7 (42.1 wt%)	35	3.5	26.2	1.8	–	–	14.9	–	–	[135]
PBI/ZIF-7 (42.1 wt%) (mixed gas)	180	3.5	440	60.3			7.3			[135]
PBI/ZIF-8 (17.8 wt%)	35	3.5	28.5	2.2	–	–	13	–	–	[83]
PBI/ZIF-8 (20.1 wt%)	35	3.5	36.4	3	–	–	12.1	–	–	[83]
PBI/ZIF-8 (31.1 wt%)	35	3.5	82.5	6.9	–	–	12.0	–	–	[136]
PBI/ZIF-8 (31.1 wt%) (mixed gas)	230	1.0	470.5	17.9	–	–	26.3	–	–	[136]
PBI/ZIF-8 (56.1 wt%)	35	3.5	1612.8	397.6	–	–	4.1	–	–	[136]
PBI/ZIF-8 (56.1 wt%) (mixed gas)	230	1.0	2014.8	164.1			12.3			[136]
PBI/ZIF-90 (9.8 wt%)	35	3.5	12.7	0.87	–	–	14.6	–	–	[137]
PBI/ZIF-90 (24.5 wt%)	35	3.5	18.3	0.89	–	–	20.6	–	–	[137]
PBI/ZIF-90 (43.7 wt%)	35	3.5	24.5	0.98	–	–	25	–	–	[137]
PBI/ZIF-90 (43.7 wt%) (mixed gas)	180	3.5	227	16.7			13.6			[137]

Note: T, testing temperature; P, transmembrane pressure; 1 Barrer = 1×10^{-10} cm^3 (STP) cm cm^{-2} s^{-1} cm Hg^{-1}.

high-performance PBI-based MMMs is to disperse nanoparticles homogeneously in the MMMs via controlling the size and surface chemistry of particles plus optimizing membrane fabrication parameters [139].

The PBI-based MMM consisting of nanoporous silicate particles exhibited an extremely low H_2 permeability in spite of the enhanced H_2/CO_2 selectivity [133]. This may be due to the large particle size as well as the weak interactions between particles and the polymer. Another PBI/silica membrane was developed by Sadeghi et al. [134]. The membrane comprising 20 wt% silica particles showed simultaneous increments in CO_2 permeability and CO_2/N_2 selectivity possibly because of better interfacial interactions and smaller particle sizes.

Recently, a series of works on PBI/ZIF nanocomposite materials were reported for high-temperature hydrogen puri cation by Yang et al. [83,135–137]. The resultant PBI/ZIF MMMs showed very encouraging H_2/CO_2 separation performance and excellent stability under elevated temperatures due to the homogeneous microstructure and good particle–polymer interactions. The PBI/ZIF-8 (30/70 w/w%) MMM exhibited a signi cantly enhanced H_2 permeability of 105.4 Barrer and a high H_2/CO_2 selectivity of 12.3 at 35°C as compared with the pure PBI membrane with a permeability of 3.7 Barrer and a selectivity of 8.7 [136]. This performance was also far surpassing the well-known Robeson upper bound [140] and most other reported polymeric materials. Under the same testing condition, the 45/55 w/w% PBI/ZIF-90 MMM possessed a remarkable ideal H_2/CO_2 separation performance (a moderate H_2 permeability of 24.5 Barrer and a high H_2/CO_2 selectivity of 25.0) [137]. At an elevated test temperature of 230°C, the H_2/CO_2 selectivity of the 30/70 w/w% PBI/ZIF-8 MMM reached an impressive value of 26.3 with a H_2 permeability of around 470 Barrer. The highest H_2 permeability of 2015 Barrer was reported from the 60/40 w/w% PBI/ZIF-8 membrane. Mixed gas data also showed that the presence of CO or water vapor impurity in the feed gas stream did not signi cantly in uence the membrane performance at 230°C. This type of PBI-based MMMs showed great potentials for hydrogen puri cation and CO_2 capture in industrial applications such as syngas processing, integrated gasi cation combined cycle (IGCC) power plant, as well as hydrogen recovery.

19.10 CURRENT PBI PRODUCTS

Not many manufacturers provide PBI products currently in the world. PBI performance Innovations Inc. is the main global manufacturer of PBI products, including powder, solution (with DMAc as the solvent), and PBI bers in various forms. PBI bers are available as a 1.5-denier staple ber, and blends of PBI with other bers, such as Nomex aramid, high-strength aramid, cotton, and rayon, are also available. In each case, PBI contributes unique thermal, ame, and chemical resistance as well as garment comfort. Some of the current applications include protective apparel, garments, and gloves for re ghters, industrial workers, race car drivers, pilots, and astronauts; it is also used in re-blocking layers for aircraft and rocket motor insulation. Extensive ame and electric arc resistance data and test methods are provided on the PBI website [140].

Celazole PBI is a unique and highly stable linear heterocyclic polymer. In high-temperature exposure to organic chemicals, Celazole molded parts offer outstanding chemical resistance and property retention, even after extended exposures. Figure 19.36 illustrates some of these products. These Celazole stock shapes offer designers continuous temperature up to 750°F (399°C) with potential short-term exposure to 1000°F (537°C) in certain environments. Celazole is ideally suited for harsh environments ranging from oil elds to aerospace service. Some current applications include (1) rollers and pedestals for handling hot glass products; (2) seals, stem packings, and valve seals used in chemical processes; (3) insulating sprue bushings for hot runner injection molding tools; (4) xtures for semiconductor industry; and (5) ultrasonic transducer/probe tips [141].

Downloaded by [Yan Wang] at 17:51 05 January 2016

© 2016 by Taylor & Francis Group, LLC

FIGURE 19.36 Some Celazole PBI performance parts. (From Polymer Corporation's Celazole PBI brochure, Reading, PA 19612-4235.)

Downloaded by [Yan Wang] at 17:51 05 January 2016

ACKNOWLEDGMENTS

Professor Wang thanks Huazhong University of Science and Technology (grant no. 0124013041) and the National Science Foundation of China (grant no. 21306058). Dr. Yang and Professor Chung acknowledge also the nancial support from the Singapore National Research Foundation (NRF) Competitive Research Program "New Biotechnology for Processing Metropolitan Organic Wastes into Value-Added Products" (R-279-000-311-281). Prof. Chung also thanks his former Hoechst Celanese colleagues Dr. G. W. Calundann, Dr. P. Chen, Dr. E.-W. Choe, Dr. O. R. Hughes, Dr. M. Jaffe, Dr. M. Sansone, and Dr. G. Serad for providing valuable technical data, and Daniel Conrad and Steven Quance from Polymer Corporation for providing PBI marketing information.

ABBREVIATIONS

6FCoPI	6FDA-polyimide
6FDA	4,4′-Hexa uoroisopropylidene-diphthalic anhydride
AMH-3	Three-dimensionally microporous layered material
CA	Cellulose acetate
DBPBI-BuI	PBI-BuI *N*-substituted by *n*-butyl groups
DBPBI-I	PBI-I *N*-substituted by *n*-butyl groups
DBzPBI-BuI	PBI-BuI *N*-substituted by 4-*tert*-butylbenzyl groups
DBzPBI-I	PBI-I *N*-substituted by 4-*tert*-butylbenzyl groups
DMA	Dynamic mechanical analysis
DMAc	Dimethylacetamide
DMFC	Direct methanol fuel cell
DMPBI-BuI	PBI-BuI *N*-substituted by methyl groups
DMPBI-I	PBI-I *N*-substituted by methyl groups
DMSO	Dimethylsulfoxide
DPIP	Diphenylisophthalate
DSC	Differential scanning calorimeter
DSPBI-BuI	PBI-BuI *N*-substituted by methylene trimethylsilyl groups
DSPBI-I	PBI-I *N*-substituted by methylene trimethylsilyl groups
DTA	Differential thermal analysis
EG	Ethylene glycol

© 2016 by Taylor & Francis Group, LLC

FESEM	Field emission scanning electron microscopy
FFV	Fractional free volume
FTIR	Fourier transform infrared spectroscopy
HFA	Hexa uoroisopropylidene bis(benzoic acid)
HIP	Hot isostatic pressing
HMA	High-modulus polyaramide
IGCC	Integrated gasi cation combined cycle
IPA	Isophthalic acid
IV	Intrinsic viscosity
LCP	Liquid crystalline polymer
LOI	Limiting oxygen index
MDA	4,4′-Methylenedianiline
MEA	Membrane electrode assembly
MMM	Mixed-matrix membrane
MP	Melting point
***m*-PBI**	Poly(2,2′-*m*-phenylene-5,5′-bibenzimidazole)
NASA	National Aeronautics and Space Administration
NF	Nano ltration
NMP	1-Methyl-2-pyrrolidinone
ODA	4,4′-Oxydianiline
OsO_4	Osmium tetroxide
PA	Phosphoric acid
PAI	Polyamideimide
PALS	Positron annihilation lifetime spectroscopy
PAMH	Proton-exchanged AMH-3
PAr	Polyarylate
PBA	Poly(1,4-benzamide)
PBI	Polybenzimidazole
PBI–2,6Py	PBI based on 3,3′-diaminobenzidine and 2,6-pyridinedicarboxylic acid
PBI–BrT	PBI based on 3,3′-diaminobenzidine and 2-bromoterephthalic acid
PBI–BuI	PBI based on 3,3′-diaminobenzidine and 5-*tert*-butylisophthalic acid
PBI–DBrT	PBI based on 3,3′-diaminobenzidine and 2,5-dibromoterephthalic acid
PBI–HFA	PBI based on 3,3′-diaminobenzidine and 3,3′-(hexa uoroisopropylidene) bis(benzoic acid)
PBI-I	PBI based on 3,3′-diaminobenzidine and isophthalic acid
PBI-T	PBI based on 3,3′-diaminobenzidine and terephthalic acid
PBZT	Poly(*p*-phenylenebenzobisthiazole)
PEEK	Polyetheretherketone
PEI	Polyetherimide
PEM	Polymer electrolyte membrane
PI	Polyimide
PPA	Polyphosphoric acid
PPS	Polyphenylene sul de
PPTA	Poly(1,4-phenyleneterephthalamide)
PRU	Polymer repeat unit
PSF	Polysulfone
PVPy	Poly(4-vinyl pyridine)
RO	Reverse osmosis
SAMH	Swollen AMH-3

Downloaded by [Yan Wang] at 17:51 05 January 2016

© 2016 by Taylor & Francis Group, LLC

TAB	3,3′,4,4′-Tetraaminobiphenyl
TEM	Transmission electron microscopy
TFP	Tetra uoropropanol
TMA	Trimetallic anhydride
ZIF	Zeolitic imidazolate framework

REFERENCES

1. H. Vogel, and C. S. Marvel, Polybenzimidazoles, I, *J. Polym. Sci.* 50: 511 (1961).
2. H. Lee, D. Stoffey, and K. Neville, Polybenzimidazoles, *New Linear Polymers*, McGraw-Hill, New York, 1967, Chap. 9.
3. A. H. Frazer, *Polymer Reviews*, Vol. 17, Interscience, New York, 1968, p. 138.
4. E. W. Neuse, Aromatic polybenzimidazoles. Syntheses, properties, and applications, *Adv. Polym. Sci.* 47: 1 (1982).
5. E. D. Powers, and G. A. Serad, History and development polybenzimidazoles, *High Performance Polymers: Their Origin and Development* (R. B. Seymour and G. S. Kirshenbaum, eds.), Elsevier, New York, 1986, p. 355.
6. A. Buckley, D. Stuetz, and G. A. Serad, Polybenzimidazoles, *Encyclopedia of Polymer Science and Engineering* (J. I. Kroschwitz, ed.), Wiley, New York, 1987, p. 572.
7. P. E. Cassidy, *Thermally Stable Polymers*, Marcel Dekker, New York, 1980, p. 168.
8. J. P. Critchley, G. J. Knight, and W. W. Wright, Polybenzimidazoles, *Heat-Resistance Polymers*, Plenum Press, New York, 1983, p. 259.
9. M. Jaffe, P. Chen, E. W. Choe, T. S. Chung, and S. Makhija, High performance polymer blends, *Adv. Polym. Sci.* 117: 297 (1994).
10. E. W. Choe, Catalysts for the preparation of polybenzimidazoles, *J. Appl. Polym. Sci.* 53: 497 (1994).
11. D. J. Jones, and J. Roziere, Recent advances in the functionalisation of polybenzimidazole and polyetherketone for fuel cell applications, *J. Membr. Sci.* 185: 41 (2001).
12. Q. Li, R. He, J. O. Jensen, and N. J. Bjerrum, PBI-based polymer membranes for high temperature fuel cells—Preparation, characterization and fuel cell demonstration, *Fuel Cells* 4: 147 (2004).
13. J. A. Asensio, and P. Gomez-Romero, Recent developments on proton conducting poly(2,5-benzimidazole) (ABPBI) membranes for high temperature polymer electrolyte membrane fuel cells, *Fuel Cells* 5: 336 (2005).
14. J. Mader, L. Xiao, T. J. Schmidt, and B. C. Benicewicz, Polybenzimidazole/acid complexes as high-temperature membranes, *Fuel Cells II, Advances in Polymer Science*, Vol. 216 (G. G. Scherer, ed.), Springer-Verlag, Berlin Heidelberg, 2008, p. 63.
15. T. Fujigaya, and N. Nakashima, Fuel cell electrocatalyst using polybenzimidazole-modi ed carbon nanotubes as support materials, *Adv. Mater.* 25: 1666 (2013).
16. T. S. Chung, A critical review of polybenzimidazoles: Historical development and future R & D, *J. Macromol. Sci. Rev. M.* C37: 277 (1997).
17. T. D. Dang, N. Venkat, and J. E. Mark, Rigid-rod polybenzimidazoles (PBIs): A concise review of their synthesis, properties, processing and applications, *Polyimides and Other High-Temperature Polymers: Synthesis, Characterization and Applications* (K. L. Mittal, ed.), VSP International Science Publishers, 2009, p. 145.
18. B. C. Ward, and L. P. DiSano, Polybenzimidazoles, *Engineered Material Handbook*, Vol. 2, Engineering Plastics, ASM International, (C. Dostal, ed.) Materials Park, OH, 1987, p. 147.
19. L. Leung, D. J. Williams, F. E. Karasz, and W. J. MacKnight, Miscible blends of polybenzimidazole with aromatic polyimide, *Polym. Bull.* 16: 457 (1986).
20. S. Stankovic', G. Guerra, D. J. Williams, F. E. Karasz, and W. J. MacKnight, Miscible blends of polybenzimidazole with a diisocyanate-based polyimide, *Polym. Commun.* 29: 14 (1988).
21. G. Guerra, D. J. Williams, F. E. Karasz, and W. J. MacKnight, Miscible polybenzimidazole blends with a benzophenone-based polyimide, *J. Polym. Sci. Polym. Phys.* 26: 301 (1988).
22. G. Guerra, S. Choe, D. J. Williams, F. E. Karasz, and W. J. MacKnight, Fourier transform infrared spectroscopy of some miscible polybenzimidazole/polyimide blends, *Macromolecules* 21: 231 (1988).
23. P. Musto, F. E. Karasz, and W. J. MacKnight, Hydrogen bonding in polybenzimidazole/polyimide systems: A fourier-transform infrared investigation using low-molecular-weight monofunctional probes, *Polymer* 30: 1012 (1989).

Downloaded by [Yan Wang] at 17:51 05 January 2016

© 2016 by Taylor & Francis Group, LLC

24. E. O. Stejskal, J. Schaefer, M. D. Sefcik, and R. A. McKay, Magic-angle carbon-13 nuclear magnetic resonance study of compatibility of solid polymeric blends, *Macromolecules* 14: 275 (1981).
25. S. Choe, W. J. MacKnight, and F. E. Karasz, Thermally induced phase behaviors of aromatic polybenzimidazole/polyimide blends, *Polym. Mat. Sci. Eng.* 59: 702 (1988).
26. D. L. VanderHart, G. C. Cambell, and R. M. Briber, Phase separation behavior of polybenzimidazole and polyethermide, *Macromolecules* 25: 4734 (1990).
27. G. Y. Kung, L. Y. Jiang, Y. Wang, and T. S. Chung, Asymmetric hollow bers by polyimide and polybenzimidazole blends for toluene/iso-octane separation, *J. Membr. Sci.* 360: 303 (2010).
28. E. Foldes, E. Fekete, F. E. Karasz, and B. Pukanszky, Interaction, miscibility and phase inversion in PBI/PI blends, *Polymer* 41: 975 (2000).
29. Z. L. Xu, T. S. Chung, K. C. Loh, and B. C. Lim, Polymeric asymmetric membranes made from polyetherimide/polybenzimidazole/poly(ethylene glycol) (PEI/PBI/PEG) for oil-surfactant-water separation, *J. Membr. Sci.* 158: 41 (1999).
30. T. S. Chung, and Z. L. Xu, Asymmetric hollow ber membranes prepared from miscible polybenzimidazole and polyetherimide blends, *J. Membr. Sci.* 147: 35 (1998).
31. T. K. Ahn, M. Kim, and S. Choe, Hydrogen-bonding strength in the blends of polybenzimidazole with BDTA- and DSDA-based polyimides, *Macromolecules* 30: 3369 (1997).
32. Y. Wang, S. H. Goh, and T. S. Chung, Miscibility study of Torlon polyamide-imide with Matrimid® 5218 polyimide and polybenzimidazole, *Polymer* 48: 2901 (2007).
33. T. S. Chung, and P. N. Chen Sr., Polybenzimidazole (PBI) and polyarylate blends, *J. Appl. Polym. Sci.* 40: 1209 (1990).
34. T. S. Chung, and P. N. Chen Sr., Film and membrane properties of polybenzimidazole (PBI) and polyarylate blends, *Polym. Eng. Sci.* 30: 1 (1990).
35. T. S. Chung, and F. K. Herold, High-modulus polyaramide and polybenzimidazole blend bers, *Polym. Eng. Sci.* 31: 1950 (1991).
36. T. S. Chung, F. K. Herold, and P. C. Chen Sr., Fibers from blends of PBI with polyaramide and polyarylate, *Proceedings of Fiber Producer Conf.*, Greenville, SC, May 1991, 3A-2.
37. C. Arrieta, E. David, P. Dolez, and T. Vu-Khanh, X-ray diffraction, Raman, and differential thermal analyses of the thermal aging of a Kevlar (R)-PBI blend fabric, *Polym. Compos.* 32: 362 (2011).
38. C. Arrieta, E. David, P. Dolez, and T. Vu-Khanh, Thermal aging of a blend of high-performance bers, *J. Appl. Polym. Sci*. 5: 3031 (2010).
39. H. Chedron, M. Haubs, F. Herod, A. Schneller, O. Herrmann-Schonherr, and R. Wagener, Miscible blends of PBI and polyaramides with polyvinylpyrrolidone, *J. Appl. Polym. Sci.* 53: 507 (1994).
40. S. Makhija, E. Pearce, T. K. Kwei, and F. Liu, Miscibility studies in blends of polybenzimidazole and poly(4-vinyl pyridine), *Polym. Eng. Sci.* 30: 798 (1990).
41. T. S. Chung, M. Glick, and E. Powers, PBI and polysulfone blend bers, *Polym. Eng. Sci.* 33: 1042 (1993).
42. T. S. Chung, The effect of LiCl on PBI and polysulfone blend bers, *Polym. Eng. Sci.* 34: 428 (1994).
43. T. S. Chung, C. M. Tun, K. P. Pramoda, and R. Wang, Novel hollow ber membranes with de ned unit-step morphological change, *J. Membr. Sci.* 1: 123 (2001).
44. F. S. Model, and L. A. Lee, An investigation of PBI hollow ber reverse osmosis membranes, *Org. Coat. Plast. Chem.* 32: 383 (1972).
45. F. S. Model, and L. A. Lee, PBI reverse osmosis membranes: An initial survey, *Reverse Osmosis Membrane Research* (H. K. Londale and H. E. Podall, eds.), Plenum Press, New York, 1972, p. 285.
46. F. S. Model, H. J. Davis, and P. A. Sessa, Preparation and evaluation of optimized hemodialysis membranes, Annual Report, NIH-NIAMDD-73-2200, U. S. Dept. of Health, Education and Welfare, 1973.
47. O. R. Hughes, P. N. Chen, W. M. Cooper, L. P. DiSano, E. Alvarez, and T. E. Andres, PBI powder processing to performance parts, *J. Appl. Polym. Sci.* 53: 485 (1994).
48. N. W. Brooks, R. A. Duckett, J. Rose, I. M. Ward, and J. Clements, An n.m.r. study of absorbed water in polybenzimidazole, *Polymer* 34: 4038 (1993).
49. K. C. Brinker, and I. M. Robinson, Linear polybenzimidazoles, U.S. Patent 2,895,949 (1959).
50. H. Vogel, and C. S. Marvel, Polybenzimidazoles, II, *J. Polym. Sci. A* 1: 1531 (1963).
51. A. B. Conciatori, E. C. Chenevey, T. C. Bohrer, and A. E. Prince Jr., Polymerization and spinning of PBI, *J. Appl. Polym. Sci.* 19: 49 (1967).
52. E. C. Chenevey, and A. B. Conciatori, Process for the polymerization of aromatic polybenzimidazoles, U.S. Patent 3,433,772 (1969).
53. A. E. Prince, Process for preparing polybenzimidazoles, U.S. Patent 3,551,389 (1970).
54. E. W. Neuse, and M. S. Loonat, Two-stage polybenzimidazole synthesis via poly(azomethine) intermediates, *Macromolecules* 16: 128 (1983).

Downloaded by [Yan Wang] at 17:51 05 January 2016

© 2016 by Taylor & Francis Group, LLC

55. R. A. Brand, M. Bruma, R. Kellman, and C. S. Marvel, Low-molecular-weight polybenzimidazoles from aromatic dinitriles and aromatic diamines, *J. Polym. Sci. Chem.* 16: 2275 (1978).
56. E. W. Choe, Single-stage melt polymerization process for the production of high molecular weight polybenzimidazole, U.S. Patent 4,312,976 (1982).
57. E. W. Choe, and A. B. Conciatori, Production of improved high molecular weight polybenzimidazole with tin containing catalyst, U.S. Patent 4,452,971 (1984).
58. E. W. Choe, and A. B. Conciatori, Two-stage melt production of high molecular weight polybenzimidazoles with phosphorous catalyst, U.S. Patent 4,485,232 (1984).
59. E. W. Choe, and A. B. Conciatori, Two-stage high molecular weight polybenzimidazole production with phosphorous containing catalyst, U.S. Patent 4,535,144 (1985).
60. R. W. Singleton, H. D. Noether, and J. F. Tracy, The effects of structure modi cations on the critical properties of PBI ber, *J. Polym. Sci. C* 19: 65 (1967).
61. Hoechst Celanese PBI brochure, P.O. Box 32414, Charlotte, NC 28232-9973.
62. S. S. Hosseini, M. M. Teoh, and T. S. Chung, Hydrogen separation and puri cation in membranes of miscible polymer blends with interpenetration networks, *Polymer* 49: 1594 (2008).
63. T. S. Chung, Z. L. Xu, and C. H. A. Huan, Halo formation in asymmetric polyetherimide and polybenzimidazole blend hollow ler membranes, *J. Polym. Sci. Pol. Phys.* 37: 1575 (1999).
64. P. Musto, F. E. Karasz, and W. J. MacKnight, Hydrogen bonding in polybenzimidazole/polyimide blends: A spectroscopic study, *Macromolecules* 24: 4762 (1991).
65. S. Choe, and T. K. Ahn, Thermally induced phase behaviors of aromatic polybenzimidazole/polyimide blends, *Polym. Mat. Sci. Eng.* 65: 331 (1991).
66. J. Grobelny, D. M. Rice, F. E. Karasz, and W. J. MacKnight, High-resolution solid state carbon-13 nuclear magnetic resonance study of polybenzimidazole/polyimide blends, *Macromolecules* 23: 2139 (1990).
67. M. Takayanagi, T. Ogata, M. Morikawa, and T. Kai, Polymer composites of rigid and exible molecules: System of wholly aromatic and aliphatic polyamides, *J. Macromol. Sci. Phys.* B17: 591 (1980).
68. W. F. Hwang, D. R. Wiff, and C. Verschoore, Phase relationship of rigid rod polymer/ exible coil polymer/solvent ternary systems, *Polym. Eng. Sci.* 23: 784 (1983).
69. W. F. Hwang, D. R. Wiff, C. L. Benner, and T. E. Helminiak, Composites on a molecular level: Phase relationships, processing, and properties, *J. Macromol. Sci. Phys.* B22: 231 (1983).
70. W. F. Hwang, D. R. Wiff, C. Verschoore, G. E. Price, T. E. Helminiak, and W. W. Adams, Solution processing and properties of molecular composite bers and lms, *Polym. Eng. Sci.* 23: 789 (1983).
71. T. E. Helminiak, C. L. Benner, F. E. Arnold, and G. E. Husman, Aromatic heterocyclic polymer alloys and products produced therefrom, U.S. Patent 4,207,407 (1980).
72. T. E. Helminiak, Air Force rigid-rod polymer bers and molecular composites, *Proceedings of Fiber Producer Conf.*, Greenville, SC, May 1991, 4B-2.
73. F. E. Arnold Jr., and F. E. Arnold, Rigid-rod polymers and molecular composites, *Adv. Polym. Sci.* 117: 257 (1994).
74. J. L. Kardos, and J. Raisoni, The potential mechanical response of macromolecular systems: A composite analogy, *Polym. Eng. Sci.* 15: 183 (1975).
75. G. Genc, B. Alp, D. Balkose, S. Ulku, and A. Cireli, Moisture sorption and thermal characteristics of polyaramide blend fabrics, *J. Appl. Polym. Sci.* 1: 29 (2006).
76. B. B. Ward, Effects of molecular weight and cure cycle on the properties of compress molded Celazole PBI resin, *Proceedings of the 32nd SAMPE Symposium*, Society for the Advancement of Material and Process Engineering, 1987, p. 853.
77. B. B. Ward, Molded Celazole PBI resin: Performance properties and aerospace-related applications, *Proceedings of the 33rd SAMPE Symposium*, Society for the Advancement of Material and Process Engineering, 1988, p. 146.
78. C. Delano, Polybenzimidazoles matrix resin and composites, *International Encyclopedia of Composites*, Vol. 6 (S. M. Lee, ed.), VCH, New York, p. 279.
79. Y. H. Lu, J. M. Chen, H. X. Cui, and H. D. Zhou, Doping of carbon ber into polybenzimidazole matrix and mechanical properties of structural carbon ber-doped polybenzimidazole composites, *Compos. Sci. Technol.* 68: 3278 (2008).
80. V. Datsyuk, S. Trotsenko, and S. Reich, Carbon-nanotube-polymer nano bers with high thermal conductivity, *Carbon* 52: 605 (2013).
81. F. J. Fu, S. Zhang, S. P. Sun, K. Y. Wang, and T. S. Chung, POSS-containing delamination-free dual-layer hollow ber membranes for forward osmosis and osmotic power generation, *J. Membr. Sci.* 443: 144 (2013).

Downloaded by [Yan Wang] at 17:51 05 January 2016

© 2016 by Taylor & Francis Group, LLC

82. J. S. Kim, and D. H. Reneker, Mechanical properties of composites using ultra ne electrospun bers, *Polym. Compos.* 20: 1124 (1999).
83. T. X. Yang, G. M. Shi, and T. S. Chung, Symmetric and asymmetric zeoliticimidazolate frameworks (ZIFs)/polybenzimidazole (PBI) nanocomposite membranes for hydrogen puri cation at high temperatures, *Adv. Energy. Mater.* 2: 1358 (2012).
84. N. Iwamoto, A property trend study of polybenzimidazole using molecular modeling, *Polym. Eng. Sci.* 34: 434 (1994).
85. National Petroleum Council, Hard truths: Facing hard truths about energy, http://downloadcenter.connectlive.com/events/npc071807/pdf-downloads/NPC-Hard_Truths-Ch2-Supply.pdf.
86. Alternative Energy, Alternative energy solutions for the 21st century, http://www.altenergy.org/.
87. H. Zhang, and P. K. Shen, Recent development of polymer electrolyte membranes for fuel cells, *Chem. Rev.* 112: 2780 (2012).
88. B. C. H. Steele, Material science and engineering: The enabling technology for the commercialisation of fuel cell systems, *J. Mater. Sci.* 36: 1053 (2001).
89. M. Molleo, T. Schmidt, and B.C. Benicewicz, Polybenzimidazole fuel cell technology: Theory, performance, and applications, *Encyclopedia of Sustainability, Science and Technology* (R. A. Meyers, ed.), Springer Science+Business Media, New York, 2012.
90. H. Ekström, B. La tte, J. Ihonen, H. Markusson, P. Jacobsson, A. Lundblad, P. Jannasch, and G. Lindbergh, Evaluation of a sulfophenylated polysulfone membrane in a fuel cell at 60 to 110 °C, *Solid State Ionics* 178: 959 (2007).
91. Q. Li, R. He, J. O. Jensen, and N. J. Bjerrum, Approaches and recent development of polymer electrolyte membranes for fuel cells operating above 100°C, *Chem. Mater.* 15: 4896 (2003).
92. S. R. Samms, S. Wasmus, and R. F. Savinell, Thermal stability of proton conducting acid doped polybenzimidazole in simulated fuel cell environments, *J. Electrochem. Soc.* 143: 1225 (1996).
93. L. Xiao, H. Zhang, E. Scanlon, L. S. Ramanathan, E.-W. Choe, D. Rogers, T. Apple, and B. C. Benicewicz, High-temperature polybenzimidazole fuel cell membranes via a sol−gel process, *Chem. Mater.* 17: 5328 (2005).
94. J. A. Asensio, E. M. Sanchez, and P. Gomez-Romero, Proton-conducting membranes based on benzimidazole polymers for high-temperature PEM fuel cells. A chemical quest, *Chem. Soc. Rev.* 39: 3210 (2010).
95. D. Mecerreyes, H. Grande, O. Miguel, E. Ochoteco, R. Marcilla, and I. Cantero, Porous polybenzimidazole membranes doped with phosphoric acid: Highly proton-conducting solid electrolytes, *Chem. Mater.* 16: 604 (2004).
96. W. J. Wainright, J. T. Wang, D. Weng, R. F. Savinell, and M. Litt, Acid−doped polybenzimidazoles: A new polymer electrolyte, *J. Electrochem. Soc.* 142: L121 (1995).
97. R. Bouchet, and E. Siebert, Proton conduction in acid doped polybenzimidazole, *Solid State Ionics* 118: 287 (1999).
98. J. A. Asensio, S. Borrós, and P. Gómez-Romero, Proton-conducting polymers based on benzimidazoles and sulfonated benzimidazoles, *J. Polym. Sci. Part A* 40: 3703 (2002).
99. D. C. Seel, B. C. Benicewicz, L. Xiao, and T. J. Schmidt, High-temperature polybenzimidazole-based membranes, *Handbook of Fuel Cells*, (W. Vielstich, H. Yokokawa, H.A. Gasteiger, eds.), John Wiley & Sons, Ltd. 2009, pp. 300–312.
100. C. B. Delano, R. R. Doyle, and R. J. Milligan, *United States Air Force Materials Laboratory*, AFML-TR-74-22, 1974.
101. T.-H. Kim, T.-W. Lim, and J.-C. Lee, High-temperature fuel cell membranes based on mechanically stable para-ordered polybenzimidazole prepared by direct casting, *J. Power Sources* 172: 172 (2007).
102. S. Yu, L. Xiao, and B. C. Benicewicz, Durability studies of PBI-based high temperature PEMFCs, *Fuel Cells* 8: 165 (2008).
103. S. Yu, H. Zhang, L. Xiao, E. W. Choe, and B. C. Benicewicz, Synthesis of poly(2,2′-(1,4-phenylene) 5,5′-bibenzimidazole) (para-PBI) and phosphoric acid doped membrane for fuel cells, *Fuel Cells* 9: 318 (2009).
104. J. A. Asensio, S. Borrós, and P. Gómez-Romero, Polymer electrolyte fuel cells based on phosphoric acid-impregnated poly(2,5-benzimidazole) membranes, *J. Electrochem. Soc.* 151: A304 (2004).
105. A. L. Gulledge, B. Gu, and B. C. Benicewicz, A new sequence isomer of AB-polybenzimidazole for high-temperature PEM fuel cells, *J. Polym. Sci. Part A* 50: 306 (2012).
106. W. C. Brinegar, Production of semipermeable PBI membranes, U.S. Patent 3,841,492 (1974).
107. L. C. Sawyer, and R. S. Jones, Observation on the structure of rst generation PBI reverse osmosis membranes, *J. Membr. Sci.* 20: 147 (1984).

Downloaded by [Yan Wang] at 17:51 05 January 2016

© 2016 by Taylor & Francis Group, LLC

108. E. A. Bower, and J. J. Rafalko, Process for modifying polybenzimidazole polymers with ethylene carbonate, U.S. Patent 4,599,388 (1986).
109. M. J. Sansone, *N*-Substituted polybenzimidazole polymer, U.S. Patent 4,898,917 (1990).
110. G. W. Calundann, and T. S. Chung, Fabrication of microporous PBI membranes with narrow pore size distribution, U.S. Patent 5,091,087 (1992).
111. K. Y. Wang, and T. S. Chung, Fabrication of polybenzimidazole (PBI) nano ltration hollow ber membranes for removal of chromate, *J. Membr. Sci.* 281: 307 (2006).
112. K. Y. Wang, Y. C. Xiao, and T. S. Chung, Chemically modi ed polybenzimidazole nano ltration membrane for the separation of electrolytes and cephalexin, *Chem. Eng. Sci.* 61: 5507 (2006).
113. K. Y. Wang, T. S. Chung, and J. J. Qin, Polybenzimidazole (PBI) nano ltration hollow ber membranes applied in forward osmosis process, *J. Membr. Sci.* 300: 6 (2007).
114. K. Y. Wang, Q. Yang, T. S. Chung, and R. Rajagopalan, Enhanced forward osmosis from chemically modi ed polybenzimidazole (PBI) nano ltration hollow ber membranes with a thin wall, *Chem. Eng. Sci.* 64: 1577 (2009).
115. M. J. Sansone, Process for the production of polybenzimidazole ultra ltration membranes, U.S. Patent 4,693,824 (1987).
116. Y. Wang, T. S. Chung, and M. Gruender, Sulfonated polybenzimidazole membranes for pervaporation dehydration of acetic acid, *J. Membr. Sci*. 415–416: 486 (2012).
117. Y. Wang, M. Gruender, and T. S. Chung, Pervaporation dehydration of ethylene glycol through polybenzimidazole (PBI)-based membranes. 1. Membrane fabrication, *J. Membr. Sci.* 363: 149 (2010).
118. Y. Wang, T. S. Chung, B. Neo, and M. Gruender, Processing and engineering of pervaporation dehydration of ethylene glycol via dual-layer polybenzimidazole (PBI)/polyetherimide (PEI) membranes, *J. Membr. Sci.* 378: 339 (2011).
119. G. M. Shi, Y. Wang, and T. S. Chung, Dual-layer PBI/P84 hollow bers for pervaporation dehydration of acetone, *AIChE J.* 58: 1133 (2012).
120. G. M. Shi, T. Yang, and T. S. Chung, Polybenzimidazole (PBI)/zeoliticimidazolate frameworks (ZIF-8) mixed matrix membranes for pervaporation dehydration of alcohols, *J. Membr. Sci.* 415–416: 577 (2010).
121. G. M. Shi, H. M. Chen, Y. C. Jean, and T. S. Chung, Sorption, swelling, and free volume of polybenzimidazole (PBI) and PBI/zeoliticimidazolate framework (ZIF-8) nano-composite membranes for pervaporation, *Polymer* 54: 774 (2013).
122. T. S. Chung, W. F. Guo, and Y. Liu, Enhanced matrimid membranes for pervaporation by homogenous blends with polybenzimidazole (PBI), *J. Membr. Sci*. 271: 221 (2006).
123. K. Y. Wang, T. S. Chung, and R. Rajagopalan, Dehydration of tetra uoropropanol (TFP) by pervaporation via novel PBI/BTDA-TDI/MDI co-polyimide (P84) dual-layer hollow ber membranes, *J. Membr. Sci.* 287: 60 (2007).
124. S. C. Kumbharkar, P. B. Karadkar, and U. K. Kharul, Enhancement of gas permeation properties of polybenzimidazoles by systematic structure architecture, *J. Membr. Sci.* 286: 161 (2006).
125. S. C. Kumbharkar, M. N. Islam, R. A. Potrekar, and U. K. Kharul, Variation in acid moiety of polybenzimidazoles: Investigation of physico-chemical properties towards their applicability as proton exchange and gas separation membrane materials, *Polymer* 50: 1403 (2009).
126. S. C. Kumbharkar, and U. K. Kharul, Investigation of gas permeation properties of systematically modi ed polybenzimidazoles by N-substitution, *J. Membr. Sci.* 357: 134 (2010).
127. S. C. Kumbharkar, and U. K. Kharul, New N-substituted ABPBI: Synthesis and evaluation of gas permeation properties, *J. Membr. Sci.* 360: 418 (2010).
128. S. C. Kumbharkar, and U. K. Kharul, N-substitution of polybenzimidazoles: Synthesis and evaluation of physical properties, *Eur. Polym. J.* 45: 3363 (2009).
129. S. C. Kumbharkar, and K. Li, Structurally modi ed polybenzimidazole hollow bre membranes with enhanced gas permeation properties, *J. Membr. Sci.* 415–416: 793 (2012).
130. S. S. Hosseini, and T. S. Chung, Carbon membranes from blends of PBI and polyimides for N2/CH4 and CO_2/CH_4 separation and hydrogen puri cation, *J. Membr. Sci.* 328: 174 (2009).
131. S. S. Hosseini, N. Peng, and T. S. Chung, Gas separation membranes developed through integration of polymer blending and dual-layer hollow ber spinning process for hydrogen and natural gas enrichments, *J. Membr. Sci.* 349: 156 (2010).
132. S. C. Kumbharkar, Y. Liu, and K. Li, High performance polybenzimidazole based asymmetric hollow bre membranes for H_2/CO_2 separation, *J. Membr. Sci.* 375: 231 (2011).
133. S. Choi, J. Coronas, Z. Lai, D. Yust, F. Onorato, and M. Tsapatsis, Fabrication and gas separation properties of polybenzimidazole (PBI)/nanoporous silicates hybrid membranes, *J. Membr. Sci*. 316: 145 (2008).

Downloaded by [Yan Wang] at 17:51 05 January 2016

© 2016 by Taylor & Francis Group, LLC

134. M. Sadeghi, M. A. Semsarzadeh, and H. Moadel, Enhancement of the gas separation properties of polybenzimidazole (PBI) membrane by incorporation of silica nano particles, *J. Membr. Sci.* 331: 21 (2009).
135. T. X. Yang, Y. Xiao, and T. S. Chung, Poly-/metal-benzimidazole nano-composite membranes for hydrogen puri cation, *Energy Environ. Sci.* 4: 4171 (2011).
136. T. X. Yang, and T. S. Chung, High performance ZIF-8/PBI nano-composite membranes for high temperature hydrogen separation consisting of carbon monoxide and water vapor, *Int. J. Hydrogen Energy* 38: 229 (2013).
137. T. X. Yang, and T. S. Chung, Room-temperature synthesis of ZIF-90 nanocrystals and the derived nanocomposite membranes for hydrogen separation, *J. Mater. Chem. A.* 1: 6081 (2013).
138. T. S. Chung, L. Y. Jiang, Y. Li, and S. Kulprathipanja, Mixed matrix membranes (MMMs) comprising organic polymers with dispersed inorganic llers for gas separation, *Prog. Polym. Sci.* 32: 483 (2007).
139. L. M. Robeson, The upper bound revisited, *J. Membr. Sci.* 320: 390 (2008).
140. PBI Performance Products, Inc., http://www.pbiproducts.com/polymers/products/celazole-u-series.
141. Polymer Corporation' Celazole PBI brochure, Reading, PA 19612-4235.

Downloaded by [Yan Wang] at 17:51 05 January 2016

© 2016 by Taylor & Francis Group, LLC